Complex and cascading triggering of submarine landslides and turbidity currents at volcanic islands revealed from integration of high-resolution onshore and offshore surveys

Michael A. Clare[*1], Tim Le Bas[1], David M. Price[1,2], James E. Hunt[1], David Sear[3], Matthieu J.B. Cartigny[4], Age Vellinga[2], William Symons[2], Christopher Firth[5], Shane Cronin[6]

[*]Corresponding author, email: m.clare@noc.ac.uk;
[1]National Oceanography Centre, University of Southampton Waterfront Campus, Southampton, SO14 3ZH, UK; [2]School of Ocean and Earth Science, University of Southampton, National Oceanography Centre, European Way, Southampton, SO14 3ZH, UK; [3]Department of Geography & Environment, University of Southampton, Highfield, Southampton, Hampshire SO17 1BJ, UK; [4]Department of Geography, Durham University, Durham DH1 3LY, UK; [5]Department of Earth and Planetary Sciences, Macquarie University, Sydney, Australia; [6]School of Environment, University of Auckland, Auckland, New Zealand.

Keywords: Cascading hazards, turbidity current, submarine landslide, tropical cyclone, outburst flood, volcanic island, crescentic bedforms, Strombolian volcano
Number of words: 8039**; Number of figures:** 13**; Number of tables:** 1

Abstract

Submerged flanks of volcanic islands are prone to hazards including submarine landslides that may trigger damaging tsunamis and fast-moving sediment-laden seafloor flows (turbidity currents) that break critical seafloor infrastructure. Small Island Developing States are particularly vulnerable to these hazards due to their remote and isolated nature, small size, high population densities and weak economies. Despite their vulnerability, few detailed offshore surveys exist for such islands, resulting in a geohazard 'blindspot', particularly in the South Pacific. Understanding how these hazards are triggered is important; however, pin-pointing specific triggers is challenging as most studies have been unable to link continuously between onshore and offshore environments, and focus primarily on large-scale eruptions with sudden production of massive volumes of sediment. Here we focus on a situation where volcanic sediment supply produces a long-term elevation over a "normal" regime, which is more similar to the long-term elevated sediment production cases at many sites (volcanic or not) where human-induced vegetation change over-supplies sediments to coastal margins. We address these issues by integrating the first detailed (2 m x 2 m) bathymetry data acquired from Tanna Island, Vanuatu with a combination of terrestrial remote sensing data, onshore and offshore sediment sampling, and documented historical events. Mount Yasur on Tanna has experienced low-magnitude Strombolian activity for at least the last 600 years. We find clear evidence for submarine landslides and turbidity currents, yet none of the identified triggers are related to major volcanic eruptions, in contrast to conclusions from several previous studies. Instead we find that cascades of non-volcanic events (including outburst floods with discharges of >1000 m^3/s, and tropical cyclones), that may be separated by decades, are more important for preconditioning and triggering in chronic sediment oversupply regimes such as at Tanna. We conclude with a general model for how submarine landslides and turbidity currents are triggered at volcanic and other heavily eroding mountainous islands. Our model highlights the often-ignored importance of outburst floods, non-linear responses to lands-use and climatic changes, and the complex interactions between a range of coastal and tectonic processes that may overshadow volcanic regimes.

1. Introduction

Active volcanic islands can create a variety of subaerial hazards including explosive eruptions that disrupt air transport (Gudmondsson et al., 2012), emission of gases harmful to health (Horwell and Baxter, 2006), fast-moving pyroclastic flows and lahars (Calder et al., 1999; Cronin et al., 1997), and ash falls that destroy agriculture and pollute water supplies (Wilson et al., 2012). Given their high relief in the surrounding deep ocean, the subaerial extents of volcanic islands are typically dwarfed by their submerged flanks. These submarine slopes are often affected by powerful, but unseen, sediment transport processes that can also pose a significant hazard (Watt et al., 2014). Subsea flank collapses can be prodigious in scale (>100s of km^3) and trigger damaging tsunamis (Moore et al., 1989; Keating and McGuire, 2000; Carey et al., 2001; Tappin et al., 2001; Coussens et al., 2016). Strategically important seafloor infrastructure, such as the subsea telecommunications cable network that transmits more than 95% of all digital data traffic worldwide, is vulnerable to submarine landslides or powerful sediment avalanches ('turbidity currents') that occur offshore from volcanic islands (Carter et al., 2014; Pope et al., 2017). Small Island Developing States are disproportionately vulnerable to both subaerial and submarine hazards; largely due to their remote and isolated nature, small size, high population densities at or near sea-level and weak economies (Briguglio, 1995; Pelling and Uitto, 2001; Cronin et al., 2004). Understanding the threats posed to seafloor cables is particularly important for these islands, as telecommunication links underpin many critical areas for development, including access to regional markets, overseas bank transactions and booking for tourism (ICPC, 2016). Despite their vulnerability, remarkably few detailed offshore surveys exist for Small Island Developing States in the South Pacific; largely due to geographic and economic constraints (Clare et al., 2018). Therefore the South Pacific has been identified as a "hazard blind-spot" with respect to submarine landslides and associated tsunamis (Goff and Terry, 2016). Furthermore, the link between onshore and offshore sediment transport processes, and hence, identification of the triggers for offshore hazards, is often unclear as integrated subaerial and submarine surveys are limited to relatively few volcanic islands worldwide (e.g. Casalbore et al., 2010; Babonneau et al, 2013).

The advent of modern multibeam bathymetry has enabled detailed imaging of the seafloor, thus providing insights into submarine landslides at volcanic islands (e.g. Mitchell et al., 2002). In addition to evidence of past slope failures, deep-water seafloor surveys (>25 m cell size) of active volcanoes have revealed that previously undocumented, crescentic bedforms are common in modern marine volcaniclastic systems (Wright et al., 2006; Hoffman et al., 2008; Silver et al., 2009; Gardner, 2010; Leat et al., 2010; Pope et al., 2018). These bedforms may be diagnostic of turbidity currents triggered by major, episodic volcanic events, including: i) sector or flank collapse; ii) powerful Vulcanian eruptions; or iii) sustained Plinian eruptions that can produce high-flux, sustained pyroclastic density currents (Pope et al., 2018). Past studies focussed on large and powerful scenarios, but what should we expect at locations where volcanoes erupt at lower rates or have long-term low but steady outputs? These cases are arguably most common, with large explosive volcanoes undergoing centuries or millennia of quiescence between events and many less-explosive volcanoes having regular small eruptions (e.g., throughout Vanuatu; Tonga, Solomon Islands, Papua New Guinea and New Zealand). Only one existing bathymetric study is known for a regularly erupting low-explosivity volcano (Stromboli: Aeolian Archipelago; Casalbore et al., 2010; 2014), which also reveals similar crescentic bedforms. Thus, is it plausible that crescentic bedforms offshore from volcanic islands may signify sudden catastrophic collapses that originate after long-term preconditioning and by a range of multiple possible triggering mechanisms –

volcanic or otherwise. With smaller individual eruptions known at such sites, collapse related bedforms thus may not constitute evidence for major volcanic events. Crescentic bedforms offshore from some volcanic islands have been tentatively linked to turbidity currents triggered by non-volcanic processes, such as ephemeral sediment-laden river floods that plunge directly into the sea (Babonneau et al., 2013; Quartau et al., 2018). Morphologically-similar crescentic bedforms have also been described in many other subaqueous, non-volcanic settings worldwide and have been related to a wide range of triggers, including: subaqueous delta collapses (Hughes Clarke, 2016; Clare et al., 2016); dense river-water plunging (Casalbore et al., 2017); settling of sediment from river plumes (Hizzett et al., 2018); wave and storm resuspension (Xu et al., 2004; Normandeau et al., 2016); and glacial outburst floods (Duller et al., 2008). Thus, there is a large degree of ambiguity in linking bedform morphology at volcanic islands with triggering mechanisms. One constraint to our understanding has been the challenge of acquiring detailed multibeam data in water depths of <100 m; hence, few studies have acquired data that extends shallow enough to link the subaerial volcano to offshore and of appropriate resolution to image bedforms (Casalbore et al., 2010; Quartau et al., 2018).

1.1. Aims

There is a pressing need to acquire detailed data offshore from volcanic islands to better understand the nature and triggers of offshore hazards, and the link between terrestrial and marine environments; in particular at Small Island Developing States and offshore from long-lived volcanoes. Here, we present the first detailed survey (2 m x 2 m cell size) offshore from Yasur volcano on Tanna Island, Vanuatu in the South Pacific. Typical volcanic activity at Yasur involves low-magnitude Strombolian eruptions, making it an ideal location for this study. We integrate our offshore data with existing and new onshore data to address the following specific aims. First, what is the offshore morphology of a continuously active and rapidly uplifting volcanic island, and what processes caused that morphology? We investigate whether arcuate-bight like features can be linked to slope failure, as suggested previously by Goff and Terry (2016), and whether offshore sediment transport pathways can be identified, such as the trains of crescentic bedforms observed on other volcanic islands. Second, we ask whether submarine landslides and crescentic bedforms found offshore from volcanic islands are always directly linked to major eruptive volcanic activity or flank collapses? We identify possible volcanic and non-volcanic triggers for submarine landslides and turbidity currents offshore Tanna Island based on documented historical events, and through integration of onshore and offshore analysis. Third, we ask how important is the role of cascades of events, which may be separated by decades, compared to instantaneous triggers? Finally, we outline a general model for the preconditioning and triggering of submarine landslides and turbidity currents at volcanic islands worldwide, based on insights from this and other studies.

2. Geological and physiographic setting for Tanna Island, Vanuatu

Tanna is one of 83 islands making up the 1200 km-long Vanuatu volcanic arc in the south-west Pacific (Brothelande et al., 2015; Fig. 1). Vanuatu is described as the most disaster-prone country in the South Pacific, and has been affected by a wide range of natural hazards in recent and historical times, including earthquakes, tropical cyclones and tsunamis (Meheux and Parker, 2006). Tanna was formed approximately 2.5 Ma by successive episodes of volcanism and reef growth (Carney and McFarlane, 1979). Volcanism is currently focussed on Yasur; one of the most active volcanoes in the archipelago. Yasur is a scoria cone, which formed from repeated Strombolian- and vulcanian-style eruptions that occur every few minutes. These are fed by a steady-state magma reservoir, which has been providing basaltic trachy-andesitic magma to drive eruptions at Yasur for at least the last 600 years (Nairn et al., 1988; Merle et al., 2013; Firth et al., 2014). Previous phases of volcanic activity in this vicinity were more dramatic, however. The Siwi ring fracture (Fig. 1), defines the previous limit of a compound caldera, which collapsed during at least two major ignimbrite-forming eruptions at approximately 43 ka and 3-8 ka (Firth et al., 2015). In its lower-most course, the Siwi River drains along the northern edge of the Siwi ring fracture, until it reaches Sulphur Bay where it meets a back barrier-type beach (Fig. 1). Until recently, the Siwi River fed into Lake Isiwi, which was dammed by a lava flow that was emplaced prior to 1800 A.D. (Fig. 1; Firth et al., 2015). Heavy rainfall in 2000 A.D. led to the breaching of the dam, triggering a major outburst flood that cut a new channel and flowed into Sulphur Bay (Kanas et al., 2000).

The present-day eruptive activity of Mount Yasur shows continuous low-level explosivity; however, shallow magma intrusion drives significant post-caldera uplift on Tanna which may contribute to a range of potential geohazards (Merle et al., 2013). The Yenkahe Resurgent Dome is among the fastest resurgent calderas worldwide (Merle et al., 2013), with uplift rates of 156 mm/year calculated over the last 1000 years from dating of uplifted coral terraces (Chen et al., 1995; Fig. 1). Two strong earthquakes in 1878 caused up to 12 m of co-seismic uplift at the coast by Port Resolution (Nairn et al., 1988; Merle et al., 2013). Photogrammetric surveys provide possible evidence for several subaerial collapse scars, each with estimated volumes of a few million cubic metres (Brothelande et al., 2015). Some of these potential headscars abut the coastline between Sulphur Bay and Port Resolution, and form steep, often-overhanging cliffs cut into weathered basaltic sands. Recommendations were made by Brothelande et al. (2015) to perform bathymetric surveys offshore from these features to understand whether such features, and their run-out, extend offshore. Our study focuses specifically on this area (Fig. 1 and 2) to understand the links between onshore and offshore sediment transport at a dynamic volcanic island through integration with previous land-based studies.

3. Data

A multibeam survey was performed by EGS Survey on behalf of the UK Hydrographic Office in March 2017. The survey covers an area of approximately 6.5 km x 3.2 km, and extends from the coastline to 292 m water depth (Fig. 2A). Multibeam bathymetry data were acquired using a Kongsberg EM2040 system (200 to 400 kHz range) and processed into 2 m x 2 m bins; hence features smaller than 2 m across cannot be resolved. An onshore photogrammetry survey of the distal part of the Siwi River and the beach at Sulphur Bay (approximately 900 m x 900 m composed from two flights) was performed in October 2017 using a DJI Phantom 4 unmanned aerial vehicle. Pix4Dcapture was used to predefine a flight plan at 100 m altitude. Agisoft Photoscan was used to create an orthomosaic with a pixel size of <4 cm. Offshore sediment sampling was performed using a two-disc grabber-cup (10 cm^3) mounted on a small portable Deep Trekker DTG2 Remotely Operated Vehicle (ROV) equipped with an additional high resolution camera (GoPro HERO4 silver) and deployed from the MV Escape (a 12.9 m catamaran) in October 2017. Onshore sediment samples were hand-excavated from the Siwi River during the same survey in October 2017. Sub-sampled sediment was sieved at 2 mm to remove rare over-sized particles then three aliquots of each sub-sample were taken for measuring grain size. Aliquot samples (1 g) were dispersed in 30 ml 0.05% sodium hexametaphosphate solution and shaken for 24 hours. Dispersed aliquots were analysed using a Malvern Mastersizer 2000 using laser diffraction of suspended sediment grains (10,000 counts) to measure grain size distributions. Grain size distributions were measured three times per aliquot. Aliquots showed intra-sample variations of <3%. Standard reference materials showed intra-sample variations of up to 3% and accuracy towards reference values of 1.5%. Scanning Electron Microscopy (SEM) was performed using a Hitachi TM-1000 Microscope at the British Ocean Sediment Core Research Facility (BOSCORF) on selected samples to investigate micro-textural properties of the sediments.

4. Results

4.1. Offshore morphology of the Yenkahe Resurgent Dome, Tanna Island

Analysis of bathymetric data (ground-truthed with ROV video footage) generally reveals a smooth low-lying seafloor (carbonate platform) or a rougher, textured seafloor (fringing or patch reefs) in shallow (<60 m) waters to the north-west of Sulphur Bay and offshore from Port Resolution (Fig. 2). Unlike its expression onshore, the edge of the Siwi Ring Fracture (i.e. the collapsed caldera margin) is difficult to trace offshore. Three different types of geomorphic character indicative of sediment transport are found locally overprinting the carbonate platform and into deeper water. These include: i) arcuate bight-like features and tilted or displaced blocks (Fig. 3); ii) linear gullies, which are either isolated or coalescent in form (Fig. 2); and iii) trains of crescentic bedforms within sinuous channels, locally associated with scours (Fig. 4&5). These three geomorphic characters now form the observational basis of this paper.

4.1.1. Arcuate bight-like features and tilted blocks

Steep-flanked (up to 60^{o}) arcuate bight-like features were identified locally cutting back into the carbonate platform (Fig. 3D). At least five tilted blocks occur immediately down-slope of an arcuate bight-like feature on the northern flank of the carbonate platform in Sulphur Bay (Fig. 3D). The largest of these blocks has an estimated volume of 9.29 x 10^{-6} km^3, but all were significantly smaller than the scar from which they originated. Three larger (<3.82 x 10^{-4} km^3) angular blocky features form localised prominent positive relief that deflect the course of seafloor channels (Fig. 3B,E&F). These blocky features have a low-angle, tilted upper surface (5-10^{o}), which is otherwise similar in seafloor expression to the surrounding flat-lying carbonate platform. Their flanks are often steep (up to 60^{o}) and are cut by arcuate incisions, downslope of which apron-like accumulations of roughly textured seafloor debris are found (Fig. 3C). The largest of these blocky features has an estimated volume of 2.29 x 10^{-3} km^3. The two debris aprons have estimated volumes of 1.28 x 10^{-3} km^3 and 9.67 x 10^{-4} km^3, assuming that they have a wedge-shaped cross-sectional geometry.

4.1.2. Linear gullies that lack bedforms

We observe two types of gulley morphology: i) isolated and ii) coalescent forms. *Isolated linear gullies* initiate in water depths of 20 to 30 m on the steepest slopes in the survey area (Fig. 2), with a mean slope of 9^{o} but can locally reach up to 30-40^{o} (Fig. 6A). Such slopes are immediately downslope of areas with a limited extent of fringing coral (extending no more than 130-200 m seaward from the high water mark) and with an abundance of boulders (observed from ROV dives). These gullies are most abundant on the eastern flank of Sulphur Bay; the flanks of the Yenkahe dome which is undergoing most rapid uplift (Fig. 1; Chen et al., 1995). Linear gullies are up to 500 m in length, and terminate as slope angles reduce; typically where they intersect sinuous channels. Linear gullies maintain a near-continuous width along their straight course, which ranges from 20 to 60 m. Bedforms are absent from linear gullies. *Coalescent gullies* initiate at water depths of ~50 m, to the north-east of Port Resolution, in an area of less dramatic uplift outside of the Yenkahe dome (Fig. 1&2). Similarly to isolated linear gullies, they initiate on slopes of up to 30^{o}, with a mean gradient of 10^{o} (Fig. 6A). Unlike isolated linear gullies, coalescent forms become adjoined down-slope from their initiation points, in an amphitheatre-shaped depression (Fig. 2). Another difference is that they initiate >500 m offshore from the high water mark, downslope of a more extensive patch of coral reef. Bedforms are also absent from these features.

4.1.3. Sinuous channels with crescentic bedforms

One of the most extensive bathymetric features in the survey area is a meandering channel that initiates as a series of small bedforms in 30 m water depth, immediately offshore from Siwi River at Sulphur Bay (Fig. 4), and extends to the north-east beyond the limits of the survey area (Fig. 4). Unlike linear gullies, this channel forms on much lower angle slopes (mean of 3^{o}; Fig. 6A). The channel contains abundant crescentic bedforms, which generally increase in wavelength and amplitude with increasing water depth, where the channel broadens out (to 200 m) on lower angle slopes. The bedforms show a backstepping asymmetry, featuring steep lee (down-stream) faces and lower angle back-angled stoss (up-stream) faces (Fig. 4C). The channel is also punctuated by steeper and deeper scours with gradients of up to 20 to 30 degrees on their lee (down-stream) face, and obstacle and comet structures (Stow et al., 2009) oriented parallel with the axis of the channel.

A series of channels also initiates in water depths of between 40 and 50 m, to the west of Port Resolution. These commence individually as approximately 10 m-wide channels, until they coalesce at approximately 125 m water depth to form one channel that broadens to approximately 130 m (Fig. 5). This combined channel then adjoins the single broad sinuous channel and extends beyond the limits of the survey area (Fig. 5). In common with the broad sinuous channel, these channels feature an abundance of similar back-stepping crescentic bedforms (Fig. 5C). The bedforms generally increase in size with increasing water depth; however, they locally attain lower amplitudes and wavelengths where the channel is constricted or steepened by seafloor relief. Channel orientation is strongly controlled by features that present prominent seafloor relief, such as tilted blocks.

4.2. Composition of seafloor sediments

Grain size analysis from crescentic bedforms in the submarine channel at Sulphur Bay reveals a very similar distribution to samples from the Siwi River, with clear bimodality at the most proximal location, becoming progressively finer offshore (Fig. 7). The grain size within linear gullies is distinctly different to both samples from Siwi River and crescentic bedforms offshore Sulphur Bay, showing a finer and broader grain size distribution. Transmitted light and scanning electron microscopy show that sediment is dominantly comprised of basaltic lithics with a small component of volcanic glass. Small amounts of carbonate and coralline debris are incorporated further offshore. Samples were not taken from the arcuate bight-like features, tilted blocks, nor the coalescent sinuous channels to the west of Port Resolution so no comment can be made on the seafloor sediments in those areas.

5. Discussion

We now first discuss the origin of the bathymetric features observed offshore Tanna and relate them to caldera collapse and different types of offshore sediment transport. Second, based on the evidence for slope instability offshore Tanna, we discuss whether similar features on volcanic islands worldwide represent tsunamigenic collapse of carbonate platforms. Third, we discuss the potential triggers for slope instability and turbidity currents on volcanic islands, initially focusing on the range of plausible triggering events at Tanna. We conclude by proposing a general model for their preconditioning and triggering at volcanic islands worldwide, invoking a complex interplay of both volcanic and non-volcanic processes.

5.1. Challenges in delineating the offshore extent of caldera margins at volcanic islands prone to offshore sediment transport

Caldera collapses at many volcanic islands have a distinct outer margin; the extent of which can be continuously mapped from onshore to offshore (e.g. Pantelleria, Italy; Nisyros and Santorini, Greece; Deception Island, Antarctica; Rabaul, Papua New Guinea; Aira, Japan - Walker, 1984; Nomikou et al., 2012). Such clarity is not apparent offshore Tanna, however. The submerged outline of the Siwi Ring Fracture is difficult to define (Fig. 1). The overall morphological complexity of the caldera at Tanna is probably due to its formation by at least two major caldera-collapse episodes, with other modification possible during smaller intervening eruptions (Firth et al., 2014; 2015). In addition, the northern margin of the Siwi Ring Fracture is possibly erased by the rapid uplift of the Yenkahe block, with higher uplift rates in the NE possibly “popping-out” the northern caldera margin. Resurgent calderas (pushed piston-like back up along caldera fractures) are common in submarine volcanic settings where magma rises into them following collapse (e.g., submarine Tonga arc; Graham et al., 2008), where crust is thin. They are also possible in other areas, e.g., Ischia Island off Naples is mapped as a fully resurgent caldera, where past caldera fill has been uplifted to form a steep island (Carlino et al., 2006). Furthermore, it is likely the seafloor was strongly affected by a combination of sediment deposition, transport, and slope failures in the period since caldera-formation. These processes have sculpted and reworked both the caldera margin and carbonate platform. That a feature which is so distinct onshore, can be almost entirely reworked or masked by offshore sediment transport processes, has implications for the recognition and interpretation of partially or entirely submerged caldera collapses in areas of active seafloor sediment transport processes.

5.2. Are arcuate bight-like features formed by slope failures and if so, were they single-event or multi-phase in nature?

Based on coarse resolution (>100 m) regional bathymetry, Terry and Goff (2013) identified arcuate bight-like features incised into carbonate platforms on a number of volcanic islands and atolls in the South Pacific, and proposed a submarine slope failure for their origin. They further suggested that such events may be very large in volume, and could trigger significant tsunamis if failure occurs in one displacement. Indeed, many studies of volcanic islands have revealed prodigious-volume landslides of their submerged flanks (e.g. Moore et al., 1989, Masson, 1996; Coussens et al., 2016). The high resolution bathymetry offshore Tanna reveals arcuate bight-like features cut into the carbonate platform. Much of the large-scale (>km) ‘scalloping’ of the carbonate platform is attributed here to caldera collapse, rather than slope failure. There is, however, compelling evidence of smaller-scale submarine slope failure within arcuate bights with perimeter lengths of 100s to 1000s of metres. These slope failures are superimposed on the post-caldera collapse relief (Fig. 3). We interpret the arcuate bights to the north and east of Sulphur Bay as the up-slope limit of collapse events. The tilted blocks found downslope (translated or rotated debris) are much smaller than the scars from which they originated (Fig. 3). Thus, it is likely that submarine slope failures offshore from Tanna occurred progressively, as multiple phases of small volume collapses and partially-rotated blocks ($<2.9 \times 10^{-3}$ km^3). The heterogeneous nature of the mixed carbonate platform and patch reefs into which these bights are incised presumably results in localised zones of weakness or less resistant material that may fail preferentially due to erosion, undercutting, or from external cyclic loading (e.g. earthquake, storm waves). These smaller bights are interpreted to arise from a combination of lateral unloading and retrogression during multiple phases of relatively small-scale slope collapses. Similar piecemeal failures of carbonate-dominated shelf breaks and slopes are common in the Bahama Banks, Great Barrier Reef and a number of volcanic-cored atolls in the South Indian Ocean (Jo et al., 2015; Puga-Bernabeau et al., 2013; Counts et al., 2018), suggesting that this situation may be similar for many other atolls and volcanic islands flanked by carbonate platform-reefs. The landslide-origin hypothesis for bight-like features (Terry and Goff, 2013) is generally supported by our findings; however, we suggest that landslide-related bights may form progressively in multiple stages rather than as one event. Multi-stage slope failures typically relate to a much lower tsunami hazard than one-off en-masse collapses, due to the smaller event volumes involved and the time elapsed between displacements (Hunt et al., 2013). Furthermore, without high resolution data, it may be challenging to attribute arcuate bight-like morphology to slope failure rather than caldera collapse. These complexities thus underline the importance of acquiring high resolution multi-beam bathymetry and the value of future efforts to map the offshore regions of Small Island Developing States for local and regional hazard assessments, particularly in the South Pacific.

5.3. What processes are responsible for creating gullies and submarine channels with crescentic bedforms?

The linear gullies and seafloor channels observed offshore Tanna (Fig. 2, 4 and 5) are morphologically similar to those observed in many settings worldwide where density currents transport sediment to deeper waters (e.g. Micallef and Mountjoy, 2011; Babonneau et al., 2013; Lonergan et al., 2013; Symons et al. 2016, Casalbore et al., 2016; Covault et al., 2017). In particular, the scale, morphology and grain-size of the crescentic bedforms within the sinuous channels are very similar (i.e. metres in wave height, tens of metres in wavelength, fine to coarse sand) to those where repeat seafloor surveys and direct flow monitoring have demonstrated the occurrence of density-stratified turbidity currents that undergo a series of hydraulic jumps, switching between super- and subcritical flow regimes that drive the up-stream migration of crescentic bedforms (Hughes Clarke, 2016; Normandeau et al., 2016; Hage et al., 2018). So why do linear gullies without bedforms occur, as well as channels with crescentic bedforms? Slope gradient appears to exert a strong control occur, as linear gullies have a significantly higher gradient (mean of 9-10^o; Fig. 6) than channels containing crescentic bedforms (mean of 3^o). This is in line with observations by Micallef and Mountjoy (2011) who identified a minimum slope threshold (5^o) for the formation of linear gullies, arguing that a critical bed shear stress can only be attained on such steep slopes. Quartau et al. (2018) only found linear gullies on the volcanic islands of the Madeira archipelago at slopes of >15^o. On the submarine flanks of Stromboli volcano, Casalbore et al. (2010) only observed crescentic bedforms on slopes of <5^o. We suggest therefore that both gullies and crescentic bedforms offshore Tanna were created by turbidity currents and that slope angle dictates the nature of the flow-seafloor interaction and thus the resultant morphology (Kostic, 2011; Zhong et al., 2015). But what processes were responsible for triggering these flows? Were volcanic events solely responsible? We now explore these questions.

5.4. Do gullies and crescentic bedforms on volcanic islands only result from flows triggered by major volcanic events?

Trains of crescentic bedforms occur on the submarine flanks of many volcanic islands globally, including Stromboli, Reunion Island, the Canary Islands, and islands in the Bismark, West Mariana, Kermadec, and South Sandwich island arcs (see database in Symons et al., 2016; Pope et al., 2018 and references therein). At most of these sites, it has been inferred that these seafloor features result from major volcanic events: either large-magnitude explosive eruptions, or large flank/sector collapses (Pope et al., 2018). This is highly unlikely to be the case for the features observed offshore Tanna. The most recent Plinian eruption on Tanna occurred ~3-8 ka, modifying the Siwi Caldera and emplacing widespread ignimbrite deposits. Onshore, these deposits radiate out from the Siwi Ring Fracture, but are absent within the caldera (Firth et al., 2015). Crescentic bedforms and linear gullies are found within the inferred offshore caldera margin, suggesting that they must post-date the caldera-modifying eruption. More recent volcanic activity from Yasur has involved continuous, low magnitude Strombolian and Vulcanian eruptions over at least the last 600 years. This style of activity produces high rates of sediment input into the surrounding areas with ash fall and also contributes to a large, devegetated or sparsely vegetated area downwind of the volcano. Eruptions with major flow events powerful enough to scour gullies onshore have not been recorded in the recent geological record. Sea cliffs between Sulphur Bay and Port Resolution (Fig. 8A) form the eastern margin of the rapidly uplifting Yenkahe Dome. Based on dating of uplifted coral terraces on this block (Fig. 1) by Chen et al. (1995), these cliffs have formed over the last 1-2 ka. Sea cliffs to the north of the Siwi River incise into deposits from Plinian eruptions dated at 3-8 ka and ~43 ka, hence they must also significantly pre-date the features observed at seafloor. We can therefore rule out these Plinian eruptions as a trigger and conclude that bedforms on the flanks of volcanic islands do not necessarily relate to major volcanic events. If this is the case, then what are the other plausible triggers? We now explore potential mechanisms, initially considering those that are indirectly related to volcanic activity, and then those that are unrelated (Table 1).

5.4.1. Low magnitude volcanic activity and related preconditioning effects

While the effect of major eruptive volcanic activity may not necessarily be directly responsible, the cumulative or antecedent conditions resulting from past or ongoing low magnitude volcanic activity may play a key role in preconditioning slopes to failure or setting up a successive chain of events that may trigger turbidity currents at volcanic islands. For instance, the accumulation of relatively weak and laminated volcanic deposits, and the effects of shallow hydrothermal circulation, are plausible contributing factors to promote slope instability (Brothelande et al., 2016). Dynamic topographic changes also play a potentially important role. The uplift rates calculated for the Yenkahe Dome, abutting the area between Sulphur Bay and Port Resolution are among the highest for any resurgent dome worldwide (156 mm/year), with two earthquake events in 1878 A.D. leading to up to 10 m co-seismic uplift at Port Resolution (Chen et al., 1995). Elevation differences between a hydrographic survey performed in 1840 A.D. and our 2017 A.D. survey, indicate the seafloor rose by between 2.6 m and 11.3 m in Resolution Bay (an area located east of the even more rapidly uplifting Yenkahe Dome). This equates to an average rise of 40 mm /year; however, most of the elevation change was likely due to the 1878 A.D. earthquakes as evidenced by eye witness accounts (Lawrie, 1898). These uplift events caused the subaerial exposure of parts of Resolution Bay, forming the present day Lake Eweya (Fig. 9). The coupling of relatively weak volcanic deposits and rapid uplift has been used to explain the presence of multiple onshore slope failures (Brothelande et al., 2016) and presumably explains the existence of steep, often-overhanging cliffs between Sulphur Bay and Port Resolution (Fig. 8A). Underwater ROV-video footage reveals accumulations of boulders and other debris below these cliffs on the carbonate platform (Fig. 8B), downslope of which a series of isolated linear gullies is found. Thus, cliff collapses may transition to sediment-laden density flows as they disaggregate and mix with seawater at the edge of the carbonate platform to create linear gullies.

5.4.2. The role of outburst floods – an under-appreciated hazard at volcanic islands?

Crescentic bedforms similar to those observed offshore Tanna have been identified at many non-volcanic locations where rivers directly feed submarine canyons or channels (Symons et al., 2016 and references therein). At river-fed locations, it is hypothesised that turbidity currents initiate from a number of possible mechanisms, during or shortly following periods of elevated river discharge. First, if sediment-laden river water is dense enough it may directly plunge upon entering the sea, initiating a hyperpycnal flow (Mulder et al., 2003). Second, settling from a buoyant sediment-laden river plume may settle more diffusively via a process known as convective fingering, periodically initiating turbidity currents (Parsons et al., 2001; Hizzett et al., 2018; Jazi and Wells, 2018). Third, sediment delivered by a river flood rapidly accumulates at the river mouth and periodically becomes unstable, thus triggering a delayed slope failure that initiates a turbidity current (Hughes Clarke, 2016; Clare et al., 2016). Submarine channels with crescentic bedforms occur offshore from river outflows on volcanic islands in La Reunion and the Madeira Archipelago, and have been tentatively linked to ephemeral periods of flash flooding that may trigger hyperpycnal flow (Babonneau et al. 2013; Quartau et al. 2018). This may indicate that river floods are a potential trigger; however, Pope et al. (2018) explicitly ruled out river floods as a potential explanation for the formation of crescentic bedforms on volcanic islands of the Kermadec Arc, on the basis of a small hydrologic system that prevents large-scale fluvial output to the ocean. At Tanna, we observe a submarine channel with crescentic bedforms offshore from the Siwi River, so are the two systems linked here? Grain size analysis points to a connection, given the similarities between samples hand-excavated from the river and those acquired from the submarine channel using an ROV (Fig. 7). However, analysis of satellite photography since 2001, and our new aerial photography, does not indicate a river plume (with the exception of the aftermath of Tropical Cyclone Pam as discussed in the following section), and the river discharge is generally very low (based on visual observations and the presence of a back barrier at the river outflow). Therefore, it is unlikely that the background river discharge is capable of directly triggering turbidity currents (Fig. 8C&D).

A series of events that culminated in May 2000 A.D. offers a likely mechanism for the submarine morphology (Fig. 10). In 2000 A.D., heavy rainfall triggered an outburst flood from Lake Isiwi, which was previously impounded by a tephra barrier on top of a lava flow. The lake had no regular surface water outlet. Heavy rainfall was exacerbated by the loss of storage capacity, caused by lake-wide deposition of over one metre (average of 2.3 m) thickness of sediments that were eroded from the flanks of Mount Yasur and the upper reaches of the catchment during tropical cyclone Uma in 1987 (Kanas et al., 2000). The outburst flood ran approximately along the course of the Siwi River, cutting a new channel of up to 40 m depth, until it reached the ocean at Sulphur Bay; washing several cattle and ten houses out to sea (Kanas et al., 2000). The village at Sulphur Bay was severely damaged by the outflow and was buried with up to 1.5 m of sediment (Kanas et al., 2000). Satellite data reveal that the back-barrier was breached, but reformed within at least a year.

As the outburst flood discharged to the ocean at the outflow of the Siwi River, it is a highly plausible candidate for creating the crescentic bedforms in the submarine channel at Sulphur Bay. So what were the likely flow conditions? The flood released 4.1 million m^3 of water over only two days, triggering catastrophic erosion of more than 1.1 million m^3 of sediment (Kanas et al., 2000; Firth et al., 2014). Based on these values, the flow averaged sediment concentration may have been up to 27% by volume (i.e. hyperconcentrated flow). This concentration is not unreasonable in light of estimates for glacial outbursts (‘jokulhaups’; Russell, 1993; Duller et al., 2008), and direct measurements of subaerial debris flows (up to 60% - Weirich, 1989) and remobilised tephra lahars (up to 62% - Lavigne and Thouret, 2003; Cronin et al., 1997) triggered by heavy rainfall. Sediments from the flood, visited by Shane Cronin only months after the event were sand-dominated levees alongside the river, consistent with hyperconcentrated flow. No debris-flow deposits were found. Microscope and SEM analysis of river sediments indicate dominantly basaltic lithics with some volcanic glasses that have a density of 2350-2650 kg/m^3 (Wilson et al., 2012). A 73% freshwater

($1000\ kg/m^3$) and 27% sediment mixture equates to a flow density of 1365-1446 kg/m^3. Thus, should the flow have maintained this concentration when it entered the ocean, the density of the flow would have far exceeded the 40 kg/m^3 above seawater (~1030 kg/m^3) required for hyperpycnal flow (Mulder et al., 2003). As a result the flow could have plunged directly to trigger a turbidity current; as observed from subaerial debris flows and lahars which transform into turbidity currents that last for many hours (Weirich, 1989; Mulder et al., 2003). Lahars can maintain hyperconcentrated conditions for over 40 km (Cronin et al., 1997), thus it is possible that the flow maintained this density to the coastline. Even if the flow had deposited much of the suspended sediment prior to reaching the ocean at Sulphur Bay, it is likely that this outburst flood could still have triggered a turbidity current at lower concentrations, particularly given its discharge. Analysis of a global collation of outburst floods (that also includes jokulhaups, artificial dam and moraine bursts) identified a power-law relationship between volume of water released and peak discharge (Manville, 2010; Fig. 11). On the basis of the volume released from Lake Isiwi, a peak discharge of 1000 m^3/s is estimated, with an upper bound (99th percentile) limit of 7000 m^3/s (Fig. 11). Turbidity currents (up to ~4 m/s) triggered by plume settling (with a density surfeit of <1 kg/m^3 above seawater) have been directly observed to occur frequently offshore from bedload-dominated rivers at a discharge threshold of >250 m^3/s and form similar bedforms (Bornhold et al., 1994; Hughes Clarke, 2016; Clare et al., 2016). Therefore, the estimated discharge value for the outburst flood on Tanna is more than that required for triggering turbidity currents. The discharge of the turbidity current itself is more challenging to estimate. The cross-sectional area of the submarine channels proximal to the river mouth is ~70 m^2, which equates to a bankfull discharge of between 210 m^3/s and 630 m^3/s assuming velocities of turbidity currents based on measurements at locations with similar-scale bedforms (3 m/s at Squamish Delta – Hughes Clarke, 2016; 9 m/s at Fraser Delta – Lintern et al., 2016). These approximate estimates may be supported by the localised presence of comet and tail scoured features within the sinuous channel offshore Sulphur Bay, which are similar to those associated with jokulhaups with observed peak discharges of ~1000 m^3/s; Russell, 1993).

Evidence for outburst floods is increasingly being identified on volcanic islands, where craters, calderas, or past lava flows trap water without a surface outlet (Manville, 2010; Delmelle et al., 2015). These floods are only exceeded in discharge volume by the breaching of glacial impoundments, which are the largest known terrestrial floods on Earth (Manville, 2010). Intracaldera lakes have been identified from more than 100 Holocene volcanoes, with similar water storage volumes to that of the impounded Lake Isiwi ($1\text{-}10 \times 10^6\ m^3$). Caldera lakes can be larger still, such as Lake Toba in Indonesia ($2.4 \times 10^{11}\ m^3$) or Lake Taupo in New Zealand ($6 \times 10^{10}\ m^3$, where an outburst flood had an estimated peak discharge of 17,000-35,000 m^3/s in 232 AD; Manville et al., 1999), and result in far greater discharges than estimated for the outburst flood in 2000 A.D. on Tanna (Fig. 11). While several studies have focused on the marine records of jokulhaups (e.g. Milliman et al., 1996; Maria et al., 2000; Willems et al., 2011; Gombiner et al., 2016), few have contemplated the offshore effects of outburst floods at volcanic islands. Given the high discharges involved, we suggest that such outburst floods may be an under-appreciated hazard and a potentially important mechanism for initiating long run-out turbidity currents at many volcanic islands.

5.4.3. Triggers unrelated to volcanic activity: Land use, extreme weather events and the role of climate change

While volcanic processes may often be indirectly responsible, a number of non-volcanic events are also capable of providing the sediment discharges and preconditioning required for submarine landslides and turbidity currents to occur. Changes in land cover resulting from human activities in coastal tropical catchments substantially increase suspended sediment loads to the coastal zone (e.g. by 5.5 times, Kroon et al 2012) and may dramatically increase the likelihood of hillslope failures and other terrestrial landslides (Froude and Petley, 2018). Historically, plantation growth and clearance by the arrival of humans on Pacific islands has increased sediment delivery from river systems as vegetation cover was disturbed by burning and cropping practices. Similarly, changes from forest cover to plantations or agriculture increase storm runoff (Comte et al 2012). Persistent volcanism exacerbates this, attested by tens of square kilometres of de-vegetated areas in areas affected by volcanic ash and acid rains (Cronin and Sharp, 2002) in downwind areas of volcanoes such as Yasur and Ambrym in Vanuatu.

Tropical cyclones are an important type of non-volcanic event that can enhance preconditioning or directly trigger submarine landslides or turbidity currents due to: i) storm wave-induced resuspension of shelf sediments; ii) cyclic loading of unstable slope sediments; iii) undercutting of coastal cliffs; or iv) extreme rainfall triggering sediment-laden river floods and surface water run-off that discharge to the ocean. Recent analysis of a global database of telecommunications cable breaks revealed that the Pacific Ocean is a hotspot for tropical cyclone-triggered turbidity currents (Pope et al., 2017). Multiple powerful cyclones have been documented in Vanuatu in recent years, including tropical cyclones Uma in 1987 A.D., Fran in 1993 A.D., Prema in 1993 A.D., Paula in 2001 A.D. and Ivy in 2004 A.D. (Koschiuch et al., 2017). Most recently, tropical cyclone Pam (13th March 2015) made landfall on Tanna Island, travelling at up to 270 km/hour with up to 5.3 m-high storm surges, resulting in up to $449M USD in damages. The direct impact of storm waves by events such as Pam is a further plausible explanation for downslope submarine sediment transport in the zone between Sulphur Bay and Port Resolution. Retrogressive or undercutting erosion of the steep coastal cliffs on Tanna by both storm waves and surface water run-off could result in cliff collapse and seaward transport of sediment; perhaps explaining the downslope location of linear gullies and coalescent sinuous channels. The power of such events is demonstrated by tropical cyclones on Fiji that were capable of eroding and transporting carbonate boulders (weighing up to 61 tonnes; Terry and Lau, 2018). Enhanced turbidity and the presence of a sediment-laden plume was visible around Sulphur Bay and Port Resolution from satellite photography in the days following tropical cyclone Pam, and the beach at Sulphur Bay was eroded landward by tens of metres (Fig. 8E&F). Enhanced river outflow also caused breaching of the barrier at the mouth of the Siwi River. River discharges following tropical cyclones can be orders of magnitude higher than background conditions, such as Cyclone Anne in 1988 which triggered a peak river discharge of more than 4,500 m^3/s on Grand Terre in New Caledonia (Fig. 11; Terry et al., 2008). Sediment loads during tropical cyclone floods have been recorded at 200-500 g/l in Fiji (Terry et al 2002); far exceeding normal concentrations. Thus, it is likely that tropical cyclone Pam may also have contributed to, or triggered a turbidity current that formed or modified bedforms in the submarine channel initiating in Sulphur Bay (Fig. 10). The increasing frequency of El-Nino-Southern Oscillation (ENSO) cycles due to climate change appear to be modifying the intensity of tropical cyclones, their migration tracks, and slowing the rate of their passage, which will result in increased surface water run-off and river discharge (Emanuel, 2005; Kossin et al., 2014; Lee et al., 2015; Gavey et al., 2016; Mie and Xie, 2016; Chand et al., 2017; Pope et al., 2017). Thus, we may expect such events to be a more likely preconditioning and/or triggering mechanism for submarine landslides and turbidity currents offshore from volcanic islands, at least in the Pacific.

5.5. A general model for triggering submarine landslides and turbidity currents at from volcanic islands

We found that a single triggering mechanism is often unlikely for submarine landslides and turbidity currents offshore from volcanic islands, and instead that a combination of processes is responsible. On Tanna for example, the series of cascading events that commenced with the closure of Lake Isiwi by a lava flow (pre-1800 AD), was compounded by the rising of lake base-level due to sediment in-wash during tropical cyclone Uma in 1987 A.D., and culminated in the flushing of sediment to the ocean following the outburst flood triggered by elevated rainfall in 2000 A.D. The outburst flood contributed to construction of the beach at Sulphur Bay, which was then eroded in 2015 A.D. during tropical cyclone Pam (Fig. 10). While separated by years to decades in time, these events each served to sequentially modify baseline conditions, setting up a cascade of hazards (Gill and Malamud, 2016). Similarly, the two earthquakes in 1878 A.D. that co-seismically uplifted sea cliffs by up to 12 m, made them steeper, and more prone to wave erosion during severe storms and tropical cyclones in the following decades. Cascading or compound effects of volcanic, climatic and anthropogenic factors should therefore not be overlooked for the triggering of slope failures and turbidity currents offshore from volcanic islands. Land cover and climate changes, in particular, are relatively slow processes that change the background state of the land surface and runoff regime, and may be punctuated by extreme events such as cyclones, earthquakes and eruptions. The result is likely to be a non-linear response over time for given individual or multiple drivers for increased sediment delivery to the coast. Positive-phase Interdecadal Pacific Oscillation (IPO) countries such as Vanuatu lie within the South Pacific Convergence Zone under normal conditions (Partin et al., 2013). During El-Nino, however, IPO-positive phase regions experience markedly increased tropical cyclone activity (Kuleshov et al., 2008; Toomey et al., 2013). If periods of increased land use (e.g. deforestation), or volcanic eruptions occur coincident with future enhanced El-Nino and tropical cyclone intensity (as is predicted for Vanuatu; Partin et al., 2013), we posit that the compounded increase in sediment loads from rivers discharging to the coastal zone will create a hotspot for turbidity current generation.

We now conclude with a general model of processes that may contribute to preconditioning and instantaneous triggering of submarine landslides and turbidity currents at volcanic islands (Fig. 12), that includes: (A) Processes that are directly related to volcanic activity that are mostly attributed to major eruptive or collapse events, e.g., Plinian eruptions (Manville et al., 1999; Pope et al., 2018); (B) Processes that are indirectly-related to volcanic activity that mostly relate to the preconditioning effects of past volcanism, or progressive ongoing low-magnitude events that may typify quiescent volcanoes and steady-state low-explosivity centres; and (C) Processes that are unrelated to volcanic activity, which include oceanographic and extreme weather events that can affect any type of volcanic island, but are most pronounced in tropical oceans. Each of these processes may play a contributing role in instantaneous triggering, or may continue to precondition the system to enhance the likelihood of offshore sediment transport; hence understanding those interplays is important. The role of cascading hazards may be much more important than that attributed to instantaneous events; particularly for volcanoes under constant low-explosivity conditions where climatic, oceanographic and anthropogenic processes may dominate. We highlight the potentially complex interrelationships between different processes in Fig. 13 (animated examples of feedback loops are shown in online video S1). Because of these compound and/or cascading relationships, attempting to identify one specific triggering mechanism for submarine landslides or turbidity currents is challenging, and may be impossible in many cases. Therefore, determining links between triggers and offshore sediment transport requires careful integration of onshore and marine datasets, and may require direct monitoring of changes in onshore environmental baselines as well as offshore sediment transport processes. Such monitoring is challenging, but new technologies now enable measurement of both the environmental conditions and seafloor processes, thus opening up new opportunities to better understand these complex links to improve offshore hazard assessments (Chouet, 1996; Lavigne et al., 2000; Clare et al., 2017; Zhang et al., 2018).

6. Conclusions

We presented the first detailed (2 m x 2 m) bathymetric data acquired offshore from Tanna Island Vanuatu and identified evidence for submarine slope failure and seafloor turbidity currents. These data, coupled with sediment sampling, help to address important knowledge gaps concerning seafloor hazards on Small Island Developing States in the South Pacific, and more generally on the flanks of Strombolian volcanoes, both of which are under-represented in the literature. We found that arcuate bight-like features, incised into the carbonate and reef platform, can be linked to slope collapses that occurred in multiple phases, and thus pose a lower tsunami hazard than if they occurred as one-off, larger failures. Integration of onshore and offshore surveys, with documented historical events, enabled identification of a number of potential triggers for slope failures and turbidity currents offshore Tanna. None of these triggers are related to major volcanic eruptions or collapses, in contrast to conclusions from several previous studies. One highly plausible triggering event was an outburst flood with an estimated discharge of >1000 m^3/s. We suggest that outburst floods from crater lakes, caldera lakes and lava flow-impounded features may be under-recognised triggers at many other volcanic islands. Non-volcanic processes, such as tropical cyclones, were also identified as a plausible trigger for triggering slope collapses and turbidity currents, due to storm loading and elevated river discharge to the sea. Tropical cyclones may become more important triggers at islands such as Tanna, due to global warming-induced changes to the El-Nino Southern Oscillation. Finally, we presented a general model for the triggering of submarine landslides and turbidity currents at volcanic islands, underlining the often-ignored importance of non-volcanic processes, and the complex interactions between a range of processes that may precondition the system. We propose that compounding effects, and cascading chains of events, may be more important than instantaneous triggers in many volcanic islands; particularly those in quiescent or Strombolian regimes.

Acknowledgements: Fieldwork and analysis was supported by the Commonwealth Marine Economies Program which aims to enable safe and sustainable marine economies across Commonwealth Small Island Developing States. We thank EGS Survey Ltd, Justin Jenkin and the crew of the MV Escape, Camillia Garae of the Vanuatu Department of Geology and Mines, and Douglas Kiri of the Vanuatu Environmental Science Society. We also thank the Department of Geology and Mines for support with fieldwork and logistics on Tanna. The staff of the BOSCORF are acknowledged for assistance with SEM analysis. We acknowledge NERC funding grants NE/M007138/1, NE/M017540/1, NE/P009190/1 and NE/P005780/1. MJB is supported by a Royal Society Dorothy Hodgkin Fellowship (RF1504449).

Author contributions: MAC led the research, wrote the manuscript and created the figures. All authors contributed to discussions to form the basis of this paper, and provided feedback on the manuscript and figures. TLB and DMP performed offshore and onshore fieldwork. JEH performed grain size, SEM and grain size analysis. DS assisted with analysis of outburst floods and links to river hydrology. MJB, AV and WS assisted with morphodynamic analysis. CF and SC assisted with analysis of the Lake Isiwi outburst flood and interpretation of volcanic aspects of the landscape.

Supplementary online material:

Video S1: Conceptual interplay of volcanic and non-volcanic processes on the preconditioning and triggering of offshore landslides and turbidity currents illustrated using a simple process interaction model. Model created using code at https://ncase.me/loopy/

References

Babonneau, N., Delacourt, C., Cancouët, R., Sisavath, E., Bachèlery, P., Mazuel, A., & Villeneuve, N. (2013). Direct sediment transfer from land to deep-sea: Insights into shallow multibeam bathymetry at La Réunion Island. Marine Geology, 346, 47-57.

Bornhold, B. D., Ren, P., & Prior, D. B. (1994). High-frequency turbidity currents in British Columbia fjords. Geo-Marine Letters, 14(4), 238-243.

Briguglio, L. (1995). Small island developing states and their economic vulnerabilities. World development, 23(9), 1615-1632.

Brothelande, E., Lénat, J. F., Normier, A., Bacri, C., Peltier, A., Paris, R., & Garaebiti, E. (2016). Insights into the evolution of the Yenkahe resurgent dome (Siwi caldera, Tanna Island, Vanuatu) inferred from aerial high-resolution photogrammetry. Journal of Volcanology and Geothermal Research, 322, 212-224.

Brothelande, E., Peltier, A., Got, J. L., Merle, O., Lardy, M., & Garaebiti, E. (2016). Constraints on the source of resurgent doming inferred from analogue and numerical modeling—Implications on the current feeding system of the Yenkahe dome–Yasur volcano complex (Vanuatu). Journal of Volcanology and Geothermal Research, 322, 225-240.

Calder, E. S., Cole, P. D., Dade, W. B., Druitt, T. H., Hoblitt, R. P., Huppert, H. E., & Young, S. R. (1999). Mobility of pyroclastic flows and surges at the Soufriere Hills Volcano, Montserrat. Geophysical Research Letters, 26(5), 537-540.

Caminade, P., Charlie, D., Kanoglu, U., Koshimura, S. I., Matsutomi, H., Moore, A., & Takahashi, T. (2000). Vanuatu earthquake and tsunami cause much damage, few casualties. EOS, Transactions American Geophysical Union, 81(52), 641-647.

Carey, S., Morelli, D., Sigurdsson, H., & Bronto, S. (2001). Tsunami deposits from major explosive eruptions: an example from the 1883 eruption of Krakatau. Geology, 29(4), 347-350.

Carlino, S., Cubellis, E., Luongo, G. and Obrizzo, F. (2006) On the mechanics of caldera resurgence of Ischia Island (southern Italy). Geological Society, London, Special Publications, 269, 181-193, doi.org/10.1144/GSL.SP.2006.269.01.12

Carney, J. N., & Macfarlane, A. (1979). Geology of Tanna, Aneityum, Futuna and Aniwa. New Hebrides Government.

Carter, L., Gavey, R., Talling, P. J., & Liu, J. T. (2014). Insights into submarine geohazards from breaks in subsea telecommunication cables. Oceanography, 27(2), 58-67.

Casalbore, D., Chiocci, F. L., Mugnozza, G. S., Tommasi, P., & Sposato, A. (2011). Flash-flood hyperpycnal flows generating shallow-water landslides at Fiumara mouths in Western Messina Strait (Italy). Marine Geophysical Research, 32(1-2), 257.

Casalbore, D., Ridente, D., Bosman, A., & Chiocci, F. L. (2017). Depositional and erosional bedforms in Late Pleistocene-Holocene pro-delta deposits of the Gulf of Patti (southern Tyrrhenian margin, Italy). Marine Geology, 385, 216-227.

Casalbore, D., Romagnoli, C., Bosman, A., & Chiocci, F. L. (2014). Large-scale seafloor waveforms on the flanks of insular volcanoes (Aeolian Archipelago, Italy), with inferences about their origin. Marine Geology, 355, 318-329.

Casalbore, D., Romagnoli, C., Chiocci, F., & Frezza, V. (2010). Morpho-sedimentary characteristics of the volcaniclastic apron around Stromboli volcano (Italy). Marine Geology, 269(3-4), 132-148.

Chand, S. S., Tory, K. J., Ye, H., & Walsh, K. J. (2017). Projected increase in El Nino-driven tropical cyclone frequency in the Pacific. Nature Climate Change, 7(2), 123.

Chen, J. K., Taylor, F. W., Edwards, R. L., Cheng, H., & Burr, G. S. (1995). Recent emerged reef terraces of the Yenkahe resurgent block, Tanna, Vanuatu: implications for volcanic, landslide and tsunami hazards. The Journal of Geology, 103(5), 577-590.

Chouet, B. A. (1996). New methods and future trends in seismological volcano monitoring. In Monitoring and mitigation of volcano hazards (pp. 23-97). Springer, Berlin, Heidelberg.

Clare, M. A., Clarke, J. H., Talling, P. J., Cartigny, M. J. B., & Pratomo, D. G. (2016). Preconditioning and triggering of offshore slope failures and turbidity currents revealed by most detailed monitoring yet at a fjord-head delta. Earth and Planetary Science Letters, 450, 208-220.

Clare, M.A., Vardy, M.E., Cartigny, M.J., Talling, P.J., Himsworth, M.D., Dix, J.K., Harris, J.M., Whitehouse, R.J. and Belal, M. (2017). Direct monitoring of active geohazards: emerging geophysical tools for deep-water assessments. Near Surface Geophysics, 15(4), pp.427-444.

Clare, M., Chaytor, J., Dabson, O., Gamboa, D., Georgiopoulou, A., Eady, H., & León, R. (2018). A consistent global approach for the morphometric characterization of subaqueous landslides. Geological Society, London, Special Publications, 477, SP477-15.

Comte, I., Colin, F., Whalen, J.K., Grünberger, O., Caliman, J-P. (2012), Agricultural Practices in Oil Palm Plantations and Their Impact on Hydrological Changes, Nutrient Fluxes and Water Quality in Indonesia: A Review. In Sparks, D.L., (Ed): Advances in Agronomy, 116,Burlington: Academic Press, 2012, pp. 71-124.

Counts, J. W., Jorry, S. J., Leroux, E., Miramontes, E., & Jouet, G. (2018). Sedimentation adjacent to atolls and volcano-cored carbonate platforms in the Mozambique Channel (SW Indian Ocean). Marine Geology, 404, 41-59.

Coussens, M., Wall-Palmer, D., Talling, P., Watt, S., Cassidy, M., Jutzeler, M., Clare, M.A., Hunt, J., Manga, M., Gernon, T. and Palmer, M. (2016). The relationship between eruptive activity, flank collapse, and sea level at volcanic islands: A long-term (> 1 Ma) record offshore Montserrat, Lesser Antilles. Geochemistry, Geophysics, Geosystems, 17(7), pp.2591-2611.

Covault, J. A., Kostic, S., Paull, C. K., Sylvester, Z., & Fildani, A. (2017). Cyclic steps and related supercritical bedforms: building blocks of deep-water depositional systems, western North America. Marine Geology, 393, 4-20.

Cronin, S. J., Gaylord, D. R., Charley, D., Alloway, B. V., Wallez, S., & Esau, J. W. (2004). Participatory methods of incorporating scientific with traditional knowledge for volcanic hazard management on Ambae Island, Vanuatu. Bulletin of volcanology, 66(7), 652-668.

Cronin, S. J., Neall, V. E., Lecointre, J. A., & Palmer, A. S. (1997). Changes in Whangaehu River lahar characteristics during the 1995 eruption sequence, Ruapehu volcano, New Zealand. Journal of volcanology and geothermal research, 76(1-2), 47-61.

Cronin, S.J., Sharp, D.S., 2002: Environmental impacts on health from continuous volcanic activity at Yasur (Tanna) and Ambrym, Vanuatu. International Journal of Environmental Health Research 12: 109-123.

Delmelle, P., Henley, R. W., & Bernard, A. (2015). Volcano-related lakes. In The Encyclopedia of Volcanoes (Second Edition) (pp. 851-864).

Duller, R. A., Mountney, N. P., Russell, A. J., & Cassidy, N. C. (2008). Architectural analysis of a volcaniclastic jökulhlaup deposit, southern Iceland: sedimentary evidence for supercritical flow. Sedimentology, 55(4), 939-964.

Emanuel, K. (2005). Increasing destructiveness of tropical cyclones over the past 30 years. Nature, 436(7051), 686.

Firth, C. W., Cronin, S. J., Turner, S. P., Handley, H. K., Gaildry, C., & Smith, I. (2015). Dynamics and pre-eruptive conditions of catastrophic, ignimbrite-producing eruptions from the Yenkahe Caldera, Vanuatu. Journal of Volcanology and Geothermal Research, 308, 39-60.

Firth, C. W., Handley, H. K., Cronin, S. J., & Turner, S. P. (2014). The eruptive history and chemical stratigraphy of a post-caldera, steady-state volcano: Yasur, Vanuatu. Bulletin of Volcanology, 76(7), 837.

Froude, M.J. and Petley, D.N. (2018). Global fatal landslide occurrence from 2004 to 2016, Natural Hazartds and Earth System Sciences, doi.org/10.5194/nhess-18-2161-2018.

Gardner, J. V. (2010). The West Mariana Ridge, western Pacific Ocean: Geomorphology and processes from new multibeam data. Bulletin, 122(9-10), 1378-1388. Gavey, R., Carter, L., Liu, J. T., Talling, P. J., Hsu, R., Pope, E., & Evans, G. (2017). Frequent sediment density flows during 2006 to 2015, triggered by competing seismic and weather events: observations from subsea cable breaks off southern Taiwan. Marine Geology, 384, 147-158.

Gill, J. C., & Malamud, B. D. (2016). Hazard interactions and interaction networks (cascades) within multi-hazard methodologies. Earth System Dynamics, 7(3), 659-679.

Goff, J., & Terry, J. P. (2016). Tsunamigenic slope failures: the Pacific Islands 'blind spot'?. Landslides, 13(6), 1535-1543.

Gombiner, J. H., Hemming, S. R., Hendy, I. L., Bryce, J. G., & Blichert-Toft, J. (2016). Isotopic and elemental evidence for Scabland Flood sediments offshore Vancouver Island. Quaternary Science Reviews, 139, 129-137.

Graham, I. J., A. G. Reyes, I. C. Wright, K. M. Peckett, I. E. M. Smith, and R. J. Arculus (2008), Structure and petrology of newly discovered volcanic centers in the northern Kermadec–southern Tofua arc, South Pacific Ocean, J. Geophys. Res., 113, B08S02, doi:10.1029/2007JB005453.

Gudmundsson, M. T., Thordarson, T., Höskuldsson, Á., Larsen, G., Björnsson, H., Prata, F. J., & Hayward, C. L. (2012). Ash generation and distribution from the April-May 2010 eruption of Eyjafjallajökull, Iceland. Scientific reports, 2, 572.

Hage, S., Cartigny, M. J., Clare, M. A., Sumner, E. J., Vendettuoli, D., Hughes Clarke, J. E., & Englert, R. G. (2018). How to recognize crescentic bedforms formed by supercritical turbidity currents in the geologic record: Insights from active submarine channels. Geology, 46(6), 563-566.

Hizzett, J. L., Hughes Clarke, J. E., Sumner, E. J., Cartigny, M. J. B., Talling, P. J., & Clare, M. A. (2018). Which Triggers Produce the Most Erosive, Frequent, and Longest Runout Turbidity Currents on Deltas?. Geophysical Research Letters, 45(2), 855-863.

Hoffmann, G., Silver, E., Day, S., Morgan, E., Driscoll, N., & Orange, D. (2008). Sediment waves in the Bismarck volcanic arc, Papua New Guinea. Special Papers-Geological Society Of America, 436, 91.

Hong, I., Pilarczyk, J. E., Horton, B. P., Fritz, H. M., Kosciuch, T. J., Wallace, D. J., & Jockley, F. R. (2018). Sedimentological characteristics of the 2015 tropical cyclone pam overwash sediments from Vanuatu, South Pacific. Marine Geology, 396, 205-214.

Horwell, C. J., & Baxter, P. J. (2006). The respiratory health hazards of volcanic ash: a review for volcanic risk mitigation. Bulletin of Volcanology, 69(1), 1-24.

Hughes Clarke, J. E. (2016). First wide-angle view of channelized turbidity currents links migrating cyclic steps to flow characteristics. Nature communications, 7, 11896.

Hunt, J. E., Wynn, R. B., Talling, P. J., & Masson, D. G. (2013). Multistage collapse of eight western Canary Island landslides in the last 1.5 Ma: Sedimentological and geochemical evidence from subunits in submarine flow deposits. Geochemistry, Geophysics, Geosystems, 14(7), 2159-2181.

Hydrographic Office of the Admiralty (1843), New Hebrides – Resolution Bay in Tanna Island, Capt. Sir E. Belcher, 1840, Chart number 1508.

International Cable Protection Committee (ICPC), (2016), Submarine Cables and BBNJ, http://www.un.org/depts/los/biodiversity/prepcom_files/ICC_Submarine_Cables_&_BBNJ_August_2016.pdf

Jazi, S. D., & Wells, M. (2018, In Press). Settling-driven convection limits the spatial scale of deposition beneath sediment-laden buoyant flows in lakes and the coastal ocean., Sedimentology, 10.31223/osf.io/9xymn

Jo, A., Eberli, G. P., & Grasmueck, M. (2015). Margin collapse and slope failure along southwestern Great Bahama Bank. Sedimentary Geology, 317, 43-52.

Kanas T, Nango I, Fransser J, Morris S (2000) Lake Siwi to River Siwi. Vanuatu Dept Land Surv 27 pp

Keating, B. H., & McGuire, W. J. (2000). Island edifice failures and associated tsunami hazards. Pure and Applied Geophysics, 157(6-8), 899-955.

Kosciuch, T. J., Pilarczyk, J. E., Hong, I., Fritz, H. M., Horton, B. P., Rarai, A., & Jockley, F. R. (2018). Foraminifera reveal a shallow nearshore origin for overwash sediments deposited by Tropical Cyclone Pam in Vanuatu (South Pacific). Marine Geology, 396, 171-185.

Kossin, J. P., Emanuel, K. A., & Vecchi, G. A. (2014). The poleward migration of the location of tropical cyclone maximum intensity. Nature, 509(7500), 349.

Kostic, S. (2011). Modeling of submarine cyclic steps: Controls on their formation, migration, and architecture. Geosphere, 7(2), 294-304.

Kroon, F.J., Kuhnert, P.M., Henderson, B.L., Wilkinson, S.N., Kinsey-Henderson, A., Abbott, B., Brodie, J.E., Turner,R.D.R. (2012). River loads of suspended solids, nitrogen, phosphorus and herbicides delivered to the Great Barrier Reef lagoon, Marine Pollution Bulletin, 65, 4, 167-181, https://doi.org/10.1016/j.marpolbul.2011.10.018.

Kuleshov, Y. L., Qui, L, Fawcett, R, Jones, D.(2008) On tropical cyclone activity in the Southern Hemisphere: Trends and the ENSO connection Geophysical Research Letters, 35.

Lawrie, J.H. (1898). Corals and Coral Islands, Transactions of the Edinburgh Field Naturalists' and Microscopical Society, volume III, p320-326.

Lavigne, F., Thouret, J. C., Voight, B., Young, K., LaHusen, R., Marso, J., & Dejean, M. (2000). Instrumental lahar monitoring at Merapi Volcano, Central Java, Indonesia. Journal of Volcanology and Geothermal Research, 100(1-4), 457-478.

Lavigne, F., & Thouret, J. C. (2003). Sediment transportation and deposition by rain-triggered lahars at Merapi Volcano, Central Java, Indonesia. Geomorphology, 49(1-2), 45-69.

Leat, P. T., Day, S. J., Tate, A. J., Martin, T. J., Owen, M. J., & Tappin, D. R. (2013). Volcanic evolution of the South Sandwich volcanic arc, South Atlantic, from multibeam bathymetry. Journal of Volcanology and Geothermal Research, 265, 60-77.

Lee, T. Y., Huang, J. C., Lee, J. Y., Jien, S. H., Zehetner, F., & Kao, S. J. (2015). Magnified sediment export of small mountainous rivers in Taiwan: chain reactions from increased rainfall intensity under global warming. PloS one, 10(9), e0138283.

Lintern, D. G., Hill, P. R., & Stacey, C. (2016). Powerful unconfined turbidity current captured by cabled observatory on the Fraser River delta slope, British Columbia, Canada. Sedimentology, 63(5), 1041-1064.

Lonergan, L., Jamin, N. H., Jackson, C. A. L., & Johnson, H. D. (2013). U-shaped slope gully systems and sediment waves on the passive margin of Gabon (West Africa). Marine Geology, 337, 80-97.

Manville, V. (2010). An overview of break-out floods from intracaldera lakes. Global and Planetary Change, 70(1-4), 14-23.

Manville, V., White, J. D. L., Houghton, B. F., & Wilson, C. J. N. (1999). Paleohydrology and sedimentology of a post–1.8 ka breakout flood from intracaldera Lake Taupo, North Island, New Zealand. Geological Society of America Bulletin, 111(10), 1435-1447.

Maria, A., Carey, S., Sigurdsson, H., Kincaid, C., & Helgadóttir, G. (2000). Source and dispersal of jokulhlaup sediments discharged to the sea following the 1996 Vatnajokull eruption. Geological Society of America Bulletin, 112(10), 1507-1521.

Masson, D. G. (1996). Catastrophic collapse of the volcanic island of Hierro 15 ka ago and the history of landslides in the Canary Islands. Geology, 24(3), 231-234.

Meheux, K., & Parker, E. (2006). Tourist sector perceptions of natural hazards in Vanuatu and the implications for a small island developing state. Tourism Management, 27(1), 69-85.

Mei, W., & Xie, S. P. (2016). Intensification of landfalling typhoons over the northwest Pacific since the late 1970s. Nature Geoscience, 9(10), 753-757.

Merle, O., Brothelande, E., Lénat, J. F., Bachèlery, P., & Garaébiti, E. (2013). A structural outline of the Yenkahe volcanic resurgent dome (Tanna Island, Vanuatu Arc, South Pacific). Journal of Volcanology and Geothermal Research, 268, 64-72.

Milliman, J. D., Snow, J., Jaeger, J., & Nittrouer, C. A. (1996). Catastrophic discharge of fluvial sediment to the ocean: evidence of Jökulhlaups events in the Alsek Sea Valley, southeast Alaska (USA). IAHS Publications-Series of Proceedings and Reports-Intern Assoc Hydrological Sciences, 236, 367-380.

Meheux, K., & Parker, E. (2006). Tourist sector perceptions of natural hazards in Vanuatu and the implications for a small island developing state. Tourism Management, 27(1), 69-85.

Micallef, A., & Mountjoy, J. J. (2011). A topographic signature of a hydrodynamic origin for submarine gullies. Geology, 39(2), 115-118.

Mitchell, N. C., Masson, D. G., Watts, A. B., Gee, M. J., & Urgeles, R. (2002). The morphology of the submarine flanks of volcanic ocean islands: a comparative study of the Canary and Hawaiian hotspot islands. Journal of Volcanology and Geothermal Research, 115(1-2), 83-107.

Moore, J. G., Clague, D. A., Holcomb, R. T., Lipman, P. W., Normark, W. R., & Torresan, M. E. (1989). Prodigious submarine landslides on the Hawaiian Ridge. Journal of Geophysical Research: Solid Earth, 94(B12), 17465-17484.

Mulder, T., Syvitski, J. P., Migeon, S., Faugeres, J. C., & Savoye, B. (2003). Marine hyperpycnal flows: initiation, behavior and related deposits. A review. Marine and Petroleum Geology, 20(6-8), 861-882.

Nairn, I.A., Scott, B.J. and Giggenbach, W.F. (1988). Yasur volcano investigations, Vanuatu, September 1988. New Zealand Geological Survey Report, G134: 74

Nomikou, P., Carey, S., Papanikolaou, D., Bell, K. C., Sakellariou, D., Alexandri, M., & Bejelou, K. (2012). Submarine volcanoes of the Kolumbo volcanic zone NE of Santorini Caldera, Greece. Global and Planetary Change, 90, 135-151.

Normandeau, A., Lajeunesse, P., Poiré, A. G., & Francus, P. (2016). Morphological expression of bedforms formed by supercritical sediment density flows on four fjord-lake deltas of the south-eastern Canadian Shield (Eastern Canada). Sedimentology, 63(7), 2106-2129.

Partin, J. W., Quinn, T. M., Shen, C. C., Emile-Geay, J., Taylor, F. W., Maupin, C. R., Lin, K., Jackson, C. S., Banner, J. L. and Sinclair, D. J. (2013) 'Multidecadal rainfall variability in South Pacific Convergence Zone as revealed by stalagmite geochemistry.' Geology, doi:10.1130/H34718.1

Parsons, J. D., Bush, J. W., & Syvitski, J. P. (2001). Hyperpycnal plume formation from riverine outflows with small sediment concentrations. Sedimentology, 48(2), 465-478.

Pelling, M., & Uitto, J. I. (2001). Small island developing states: natural disaster vulnerability and global change. Global Environmental Change Part B: Environmental Hazards, 3(2), 49-62.

Pope, E. L., Jutzeler, M., Cartigny, M. J., Shreeve, J., Talling, P. J., Wright, I. C., & Wysoczanski, R. J. (2018). Origin of spectacular fields of submarine sediment waves around volcanic islands. Earth and Planetary Science Letters, 493, 12-24.

Pope, E. L., Talling, P. J., Carter, L., Clare, M. A., & Hunt, J. E. (2017). Damaging sediment density flows triggered by tropical cyclones. Earth and Planetary Science Letters, 458, 161-169.

Puga-Bernabéu, Á., Webster, J. M., Beaman, R. J., & Guilbaud, V. (2013). Variation in canyon morphology on the Great Barrier Reef margin, north-eastern Australia: The influence of slope and barrier reefs. Geomorphology, 191, 35-50.

Quartau, R., Ramalho, R. S., Madeira, J., Santos, R., Rodrigues, A., Roque, C., & da Silveira, A. B. (2018). Gravitational, erosional and depositional processes on volcanic ocean islands: Insights from the submarine morphology of Madeira Archipelago. Earth and Planetary Science Letters, 482, 288-299.

Russell, A. J. (1993). Obstacle marks produced by flow around stranded ice blocks during a glacier outburst flood (jökulhlaup) in west Greenland. Sedimentology, 40(6), 1091-1111.

Silver, E., Day, S., Ward, S., Hoffmann, G., Llanes, P., Driscoll, N., and Saunders, S. (2009). Volcano collapse and tsunami generation in the Bismarck volcanic arc, Papua New Guinea. Journal of Volcanology and Geothermal Research, 186(3-4), 210-222.

Stow, D. A., Hernández-Molina, F. J., Llave, E., Sayago-Gil, M., Díaz del Río, V., & Branson, A. (2009). Bedform-velocity matrix: the estimation of bottom current velocity from bedform observations. Geology, 37(4), 327-330.

Symons, W. O., Sumner, E. J., Talling, P. J., Cartigny, M. J., & Clare, M. A. (2016). Large-scale sediment waves and scours on the modern seafloor and their implications for the prevalence of supercritical flows. Marine Geology, 371, 130-148.

Tappin, D. R., Watts, P., McMurtry, G. M., Lafoy, Y., & Matsumoto, T. (2001). The Sissano, Papua New Guinea tsunami of July 1998—offshore evidence on the source mechanism. Marine Geology, 175(1-4), 1-23.

Terry, J.P., Garimella, S., Kostaschuk, R.A. (2002). Rates of floodplain accretion in a tropical island river system impacted by cyclones and large floods, Geomorphology, 42, 3–4, 171-182, https://doi.org/10.1016/S0169-555X(01)00084-8 .

Terry, J. P., & Goff, J. (2013). One hundred and thirty years since Darwin: 'Reshaping' the theory of atoll formation. The Holocene, 23(4), 615-619.

Terry, J. P., & Goff, J. R. (2012). The special vulnerability of Asia–Pacific islands to natural hazards. Geological Society, London, Special Publications, 361(1), 3-5.

Terry, J. P., Kostaschuk, R. A., & Wotling, G. (2008). Features of tropical cyclone-induced flood peaks on Grande Terre, New Caledonia. Water and Environment Journal, 22(3), 177-183.

Terry, J. P., & Lau, A. A. (2018). Magnitudes of nearshore waves generated by tropical cyclone Winston, the strongest landfalling cyclone in South Pacific records. Unprecedented or unremarkable?. Sedimentary Geology, 364, 276-285.

Toomey M., Donnelly J., Woodruff J. (2013) Reconstructing mid-late Holocene cyclone variability in the Central Pacific using sedimentary records from Tahaa, French Polynesia. Quat Sci Rev 77:181–189.

Walker, G. P. (1984). Downsag calderas, ring faults, caldera sizes, and incremental caldera growth. Journal of Geophysical Research: Solid Earth, 89(B10), 8407-8416.

Watson, S. J., Whittaker, J. M., Lucieer, V., Coffin, M. F., & Lamarche, G. (2017). Erosional and depositional processes on the submarine flanks of Ontong Java and Nukumanu atolls, western equatorial Pacific Ocean. Marine Geology, 392, 122-139.

Watt, S. F., Talling, P. J., & Hunt, J. E. (2014). New insights into the emplacement dynamics of volcanic island landslides. Oceanography, 27(2), 46-57.

Weirich, F. H. (1989). The generation of turbidity currents by subaerial debris flows, California. Geological Society of America Bulletin, 101(2), 278-291.

Willems, B. A., Powell, R. D., Cowan, E. A., & Jaeger, J. M. (2011). Glacial outburst flood sediments within Disenchantment Bay, Alaska: implications of recognizing marine jökulhlaup deposits in the stratigraphic record. Marine Geology, 284(1-4), 1-12.

Wilson, T. M., Stewart, C., Sword-Daniels, V., Leonard, G. S., Johnston, D. M., Cole, J. W., & Barnard, S. T. (2012). Volcanic ash impacts on critical infrastructure. Physics and Chemistry of the Earth, Parts A/B/C, 45, 5-23.

Wright, I. C., Worthington, T. J., & Gamble, J. A. (2006). New multibeam mapping and geochemistry of the 30–35 S sector, and overview, of southern Kermadec arc volcanism. Journal of Volcanology and Geothermal Research, 149(3), 263-296.

Xu, J. P., Noble, M. A., & Rosenfeld, L. K. (2004). In-situ measurements of velocity structure within turbidity currents. Geophysical Research Letters, 31(9).

Zhang, Y., Liu, Z., Zhao, Y., Colin, C., Zhang, X., Wang, M., & Kneller, B. (2018). Long-term in situ observations on typhoon-triggered turbidity currents in the deep sea. Geology

Zhong, G., Cartigny, M. J., Kuang, Z., & Wang, L. (2015). Cyclic steps along the South Taiwan Shoal and West Penghu submarine canyons on the northeastern continental slope of the South China Sea. Bulletin, 127(5-6), 804-824.

Table 1: Review of possible triggers for turbidity currents and submarine landslides at volcanic islands, with specific reference to documented events at Tanna Island (parenthesised numbers are cross-references to Fig. 12)

Event	Triggering mechanism	Known events on Tanna Island
Directly related to volcanic activity		
Eruption / pyroclastic flow	[1] Directly triggered as dense pyroclastic surge plunges into the sea or indirectly triggered from enhanced settling of grains by convective fingering due to [2] lofted surge cloud that overruns the sea or [3] tephra fallout from eruption cloud.	Last known pyroclastic-forming eruptions occurred at 3-8 ka and 34 ka (Firth et al., 2015) so unlikely to be responsible for features observed on present day seafloor.
Flank / dome / sector collapse	[4] Turbidity current evolves from slope failure or lava dome collapse due to eruption or growth of magma chamber.	Last major sector collapse was 34 ka so unlikely responsible for features on present day seafloor. No major collapses have occurred in recent times, but local slope failure may have been triggered due to fast uplift rates (156 mm/year, averaged over 2 ka) for the Yenkahe resurgent dome (Chen et al., 1995; Firth et al., 2015)
Indirectly related to volcanic activity		
Crater lake or lava-dammed lake outburst flood	[5] Sudden discharge of heavily sediment-laden outwash [A] plunges to directly trigger hyperpycnal flow, [B] indirectly triggers turbidity current due to settling out of sediment from a sediment-laden plume, or [C] leads to rapid accumulation of sediment at shelf break setting up delayed slope failure.	Heavy rainfall in 2000 triggered outburst flood from Lake Isiwi releasing 4.1 million m^3 of water and erosion of 1.1 million m^3 of sediment that cut a new channel and flowed out to sea at Sulphur Bay (Kanas et al., 2000; Firth et al., 2014). Estimated peak discharge of >1,000 m^3/s.
Lahar	[6] Heavy rainfall mobilises volcanic sediments and washes them offshore and triggers turbidity currents (in the same manner as 5A-C above).	No recorded evidence, but may occur due to tropical cyclone [8].
Earthquake / ground movement	[7] Ground shaking and/or uplift triggers slope or cliff collapse of weathered subaerial volcanic sediments or at the steep fringes of carbonate platform.	Strong ground movement (from witnesses) and co-seismic uplift of up to 12 m due to two earthquakes in 1878 (Chen et al.,1995).
Unrelated to volcanic activity		
Tsunami or storm surge	[8] Loading by waves triggers [A] slope instability or cliff collapse or [B] resuspension of seafloor sediments.	7.1-7.5 M_w earthquake triggered a tsunami on November 26th 1999 with 6.6 m run-up height on Tanna. Tsunamis also recorded in 1875, 1961, 1965 (Caminade et al., 2000).
Tropical cyclone	[9] Heavy rainfall triggers [A] enhanced sediment-laden surface water runoff that can trigger cliff collapse, or [B] dense river outflow that enters the sea. [C] Rapid accumulation of sediment at shelf break may lead to delayed slope failure.	Long history of cyclones at Tanna including Tropical Cyclone Pam (2015), Ivy (2004), Paula (2001), Prema (1993), Fran (1992), Uma (1987). Pam was up to 270 km/hour, up to 5.3 m maximum flow height, and triggered enhanced run-off (Hong et al., 2017).
Onshore failures / cliff collapse	[10] Onshore slope failures or collapse of coastal cliffs enters the sea triggered by climatic, erosion, or other non-volcanic processes (Terry and Goff, 2016).	Two historic landslides (1919 and 1975) occurred on the slopes of Yasur's cone but did not enter the sea (Carney and Macfarlane, 1979; Merle et al., 2013). Steep overhanging sea cliffs cut into weathered basalt may represent the headscars of subaerial failures (Brothelande et al., 2015) prone to incipient failure.

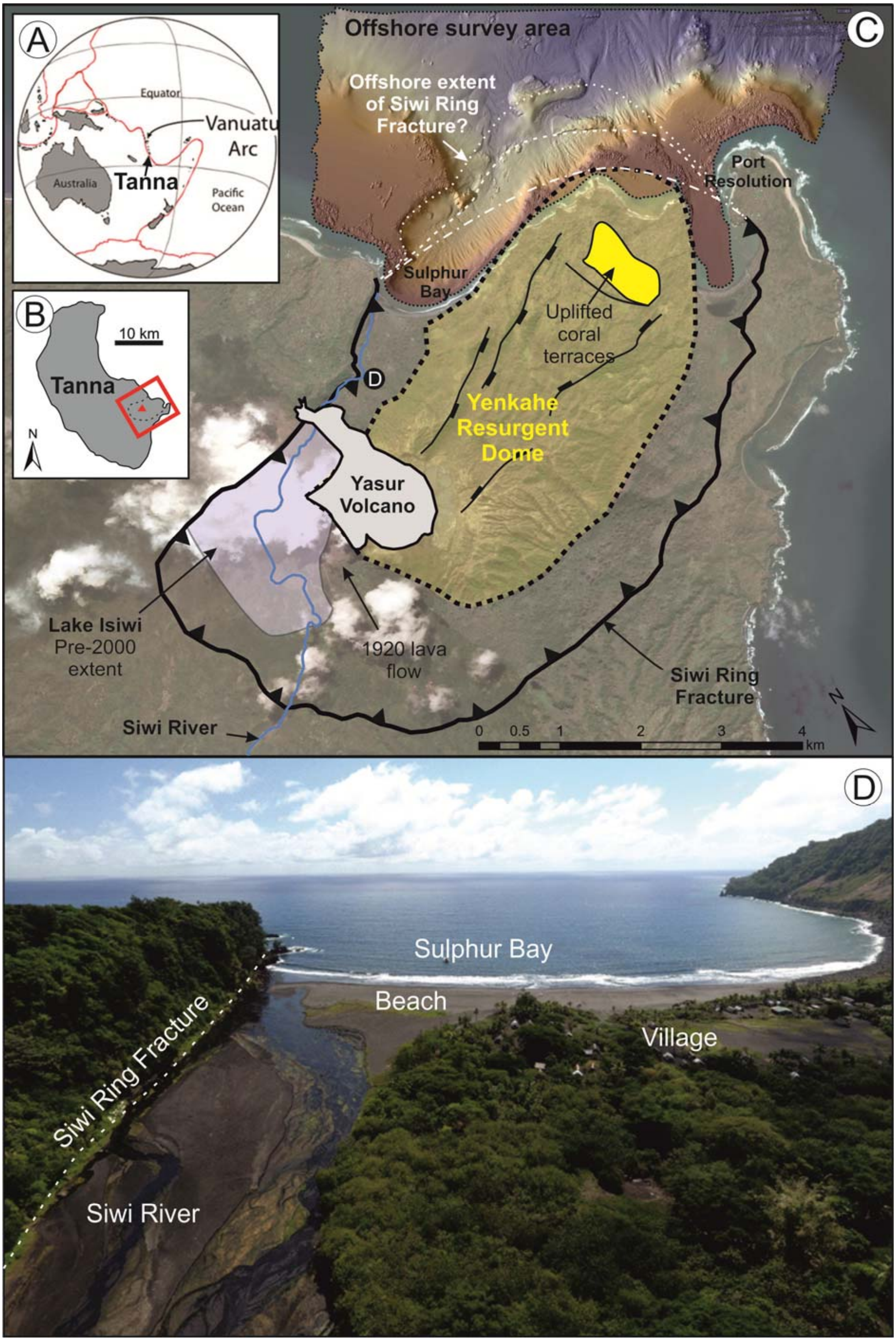
A
Equator
Vanuatu Arc
Australia
Tanna
Pacific Ocean
B
10 km
Tanna
N
C
Offshore survey area
Offshore extent of Siwi Ring Fracture?
Port Resolution
Sulphur Bay
Uplifted coral terraces
D
Yenkahe Resurgent Dome
Yasur Volcano
Lake Isiwi
Pre-2000 extent
1920 lava flow
Siwi Ring Fracture
Siwi River
0 0.5 1 2 3 4 km
N
D
Sulphur Bay
Beach
Village
Siwi Ring Fracture
Siwi River

Figure 1: (A) Location of Vanuatu Arc and (B) Tanna Island. Location and extent of survey area offshore Tanna Island, Vanuatu (C) shown in relation to onshore features. Onshore geomorphological and structural mapping based on Firth et al. (2014) and Brothelande et al (2015). Three possible locations of the offshore extent of the Siwi Ring Fracture are annotated in white. Terrestrial photography from Google: Digital Globe. Aerial drone photograph (D) of Siwi River and Sulphur Bay taken towards the north-east at point D annotated on panel C.

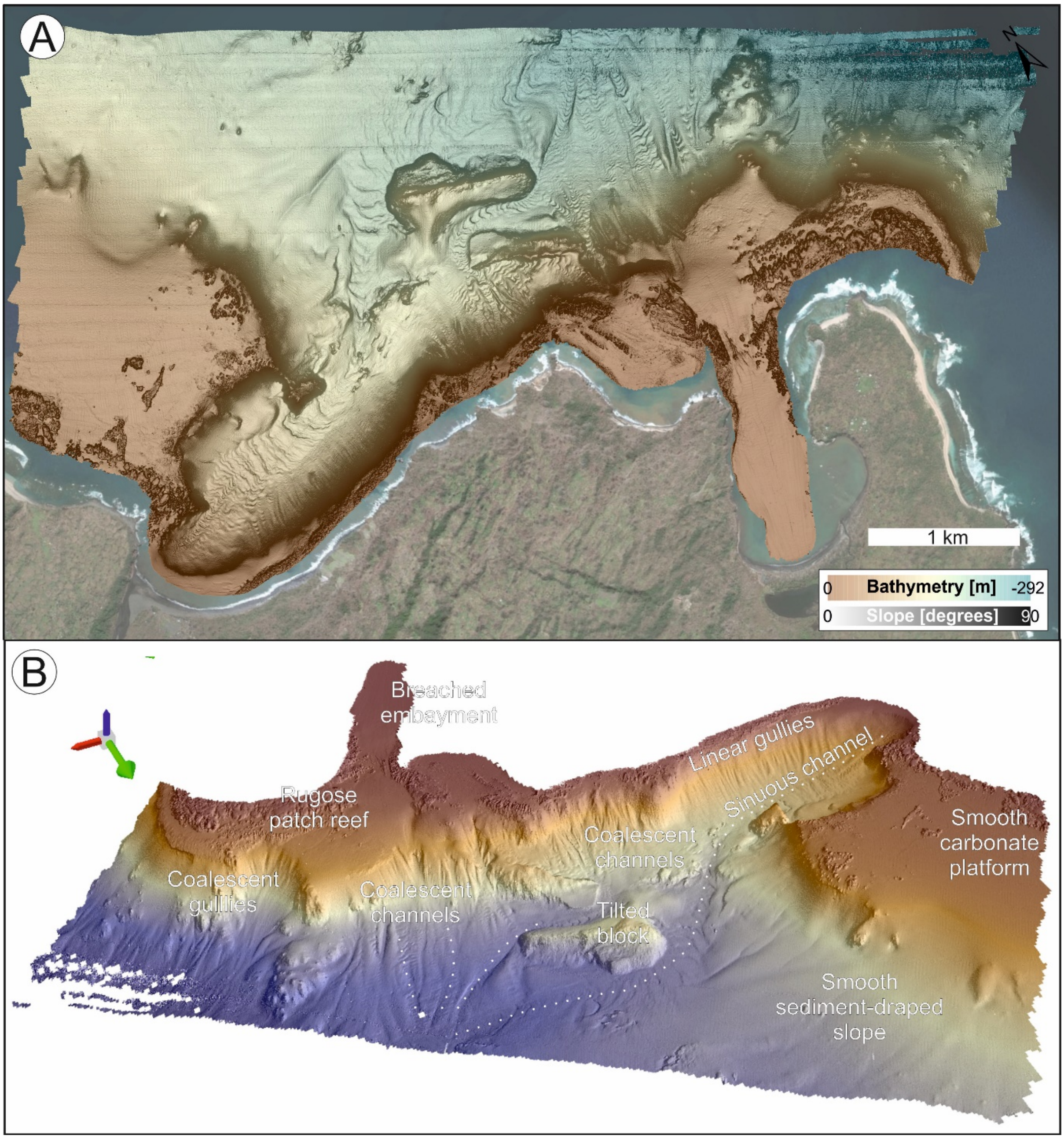

Figure 2: Overview of seafloor topography and main features in the study area. (A) Colourwash bathymetry overlain on greyscale slope map. Terrestrial data from Google: Digital Globe. (B) 3D rendering (3 x vertical exaggeration) of hillshaded bathymetry (illumination from the north-west) annotated with main geomorphologic features and north-arrow (green).

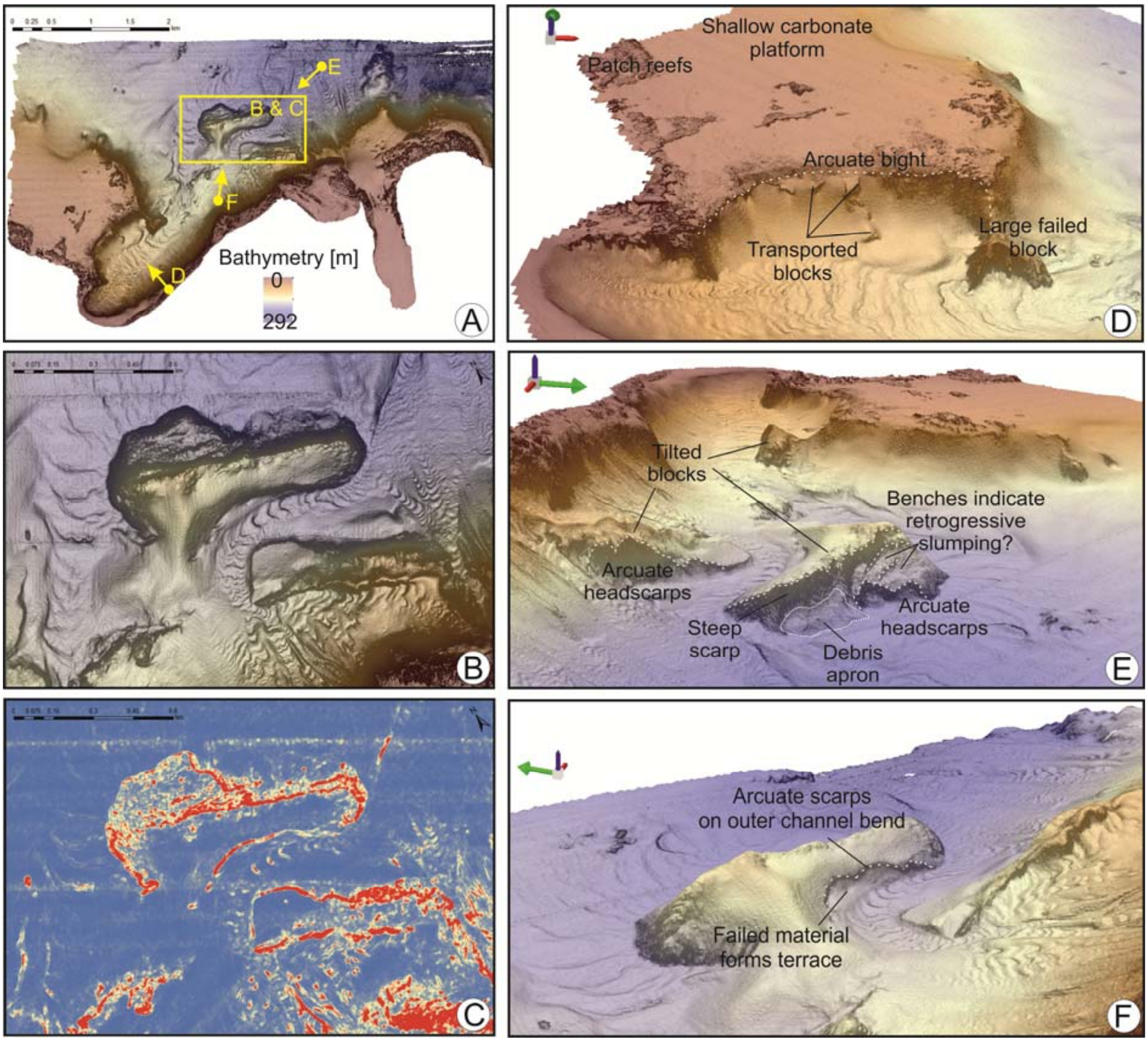

Figure 3: Overview map (A) annotated with panels that illustrate evidence for localised slope instability. Line of sight is illustrated for the following panels. Slope rendering (B, where black is steepest slope) and seafloor roughness (C, where red is roughest and blue is smoothest) maps show an elongated, tilted block that may be a failed slab of carbonate platform that has subsequently been eroded around. Arcuate bight-like structures may reflect past episodes of slope instability, and feature small blocks that appear to have slumped (D). High slope angles (B) and roughness (C) on the flanks of the elongated, tilted block may indicate smaller-scale incipient slope failures, which are annotated in 3D renderings (E and F).

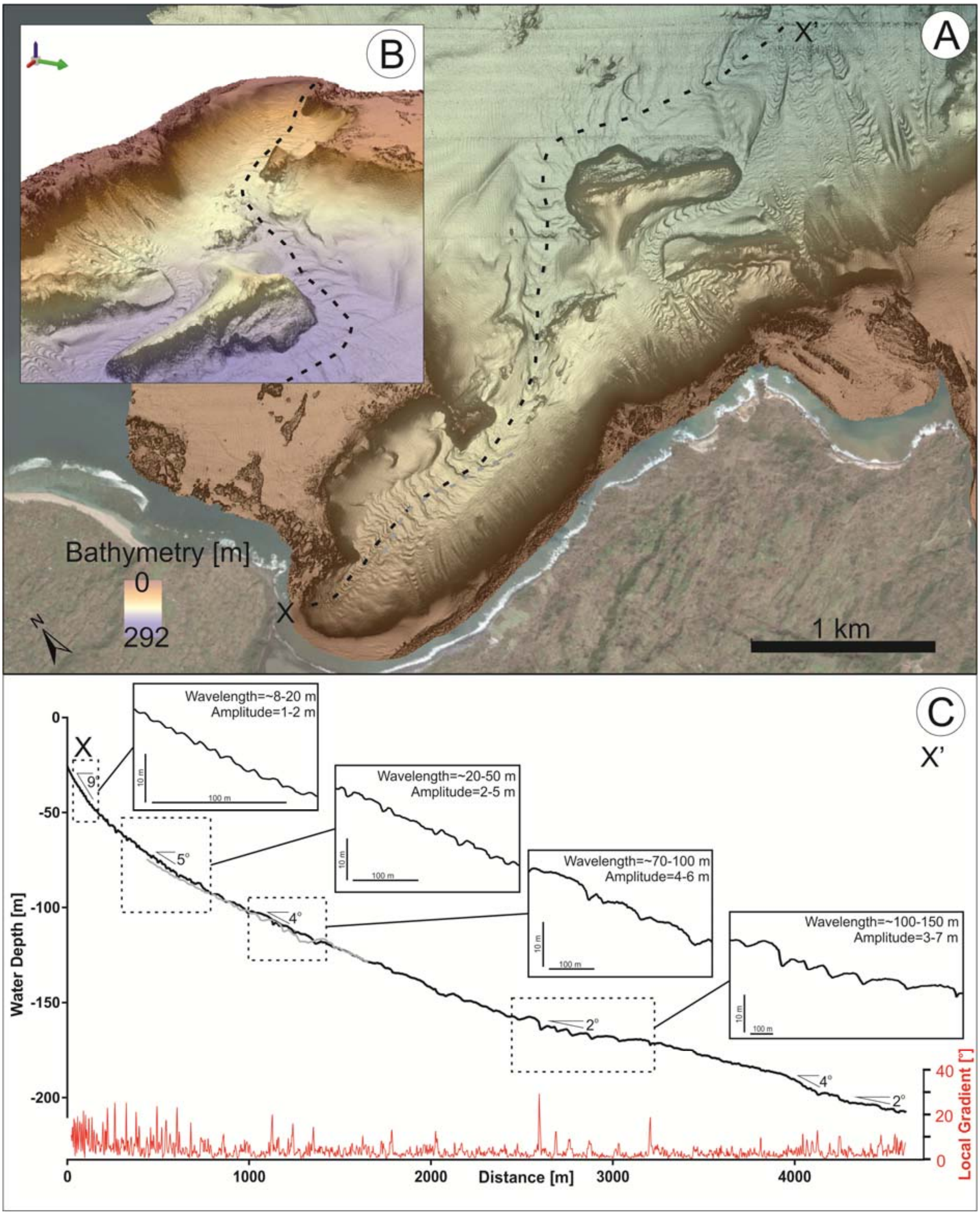

Figure 4: Overview map (A) and 3D rendering (B) annotated with dashed line along the axis of sinuous channel with cresentic bedforms that originates in Sulphur Bay. Along-channel profile (black and grey lines in C) shows how bedforms generally increase in wavelength and amplitude with increasing water depth. Average slope gradients are annotated on the black profile, while local slope gradient that highlights bedforms and knickpoints is shown as a red line in (C).

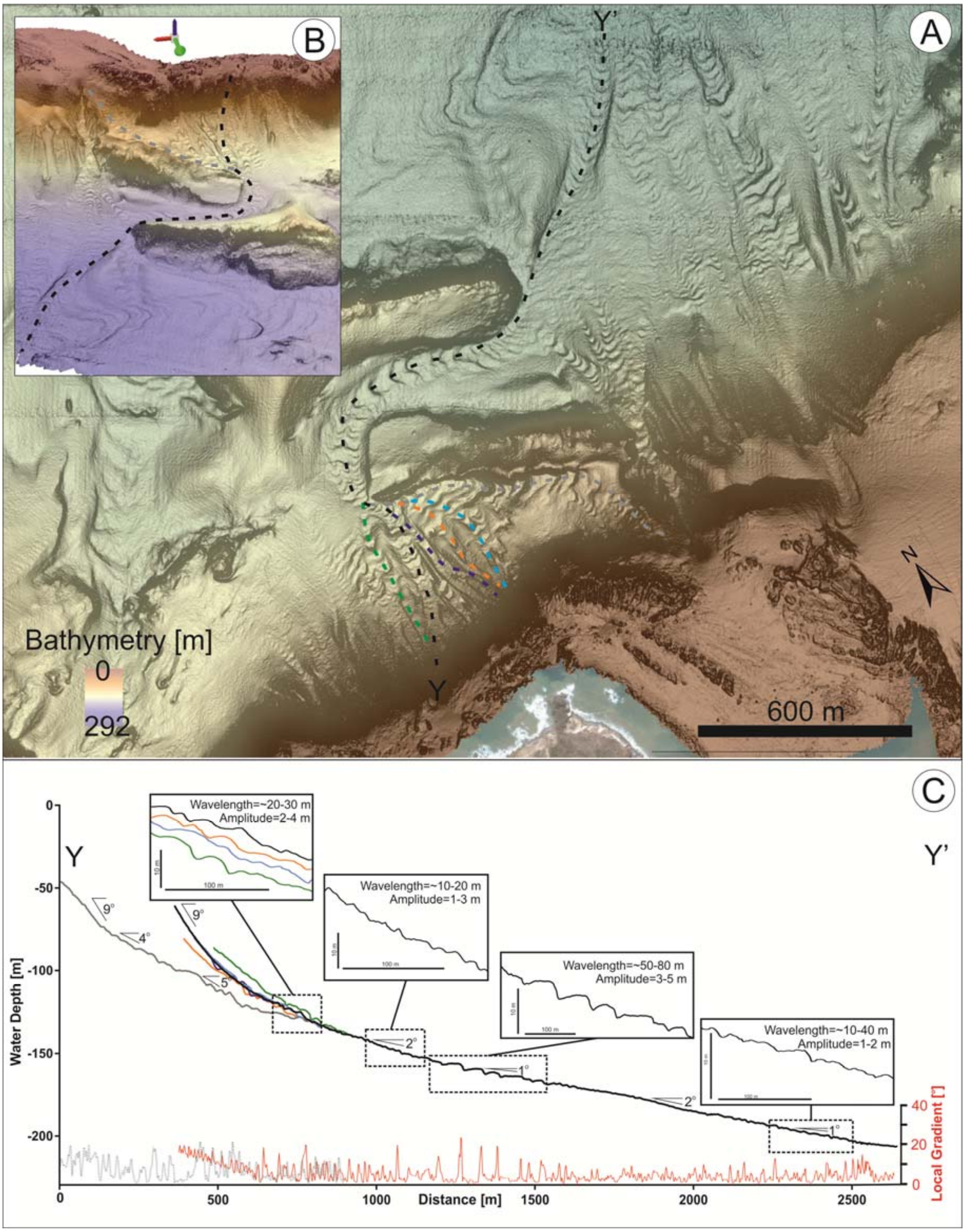

Figure 5: Overview map (A) and 3D rendering (B) annotated with dashed lines along the axis of sinuous coalescent channels with cresentic bedforms that originate ~2.5 km to the east of Sulphur Bay. Along-channel profiles (black, grey, blue, orange and green lines in C) show how bedforms generally increase in wavelength and amplitude to 1500 m water depth, but then decrease in response to the constriction of the channel. Average slope gradients are annotated on the black profile, while local slope gradient that highlights bedforms is shown as a red line in (C).

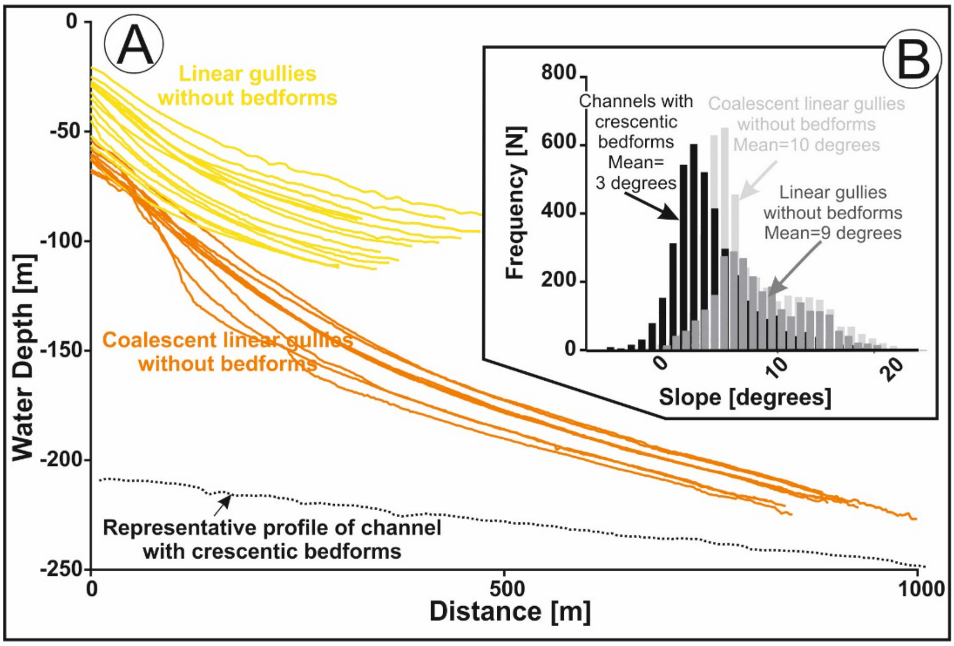

Figure 6: Isolated linear gullies are much shorter in length than coalescent gullies, but attain similar slope angles, which are higher on average than those for channels with crescentic bedforms (A). Local slope measurements along all mapped gullies and channels (B) shows that channels with crescentic bedforms only occur at much lower slope angles (mean of 3 degrees).

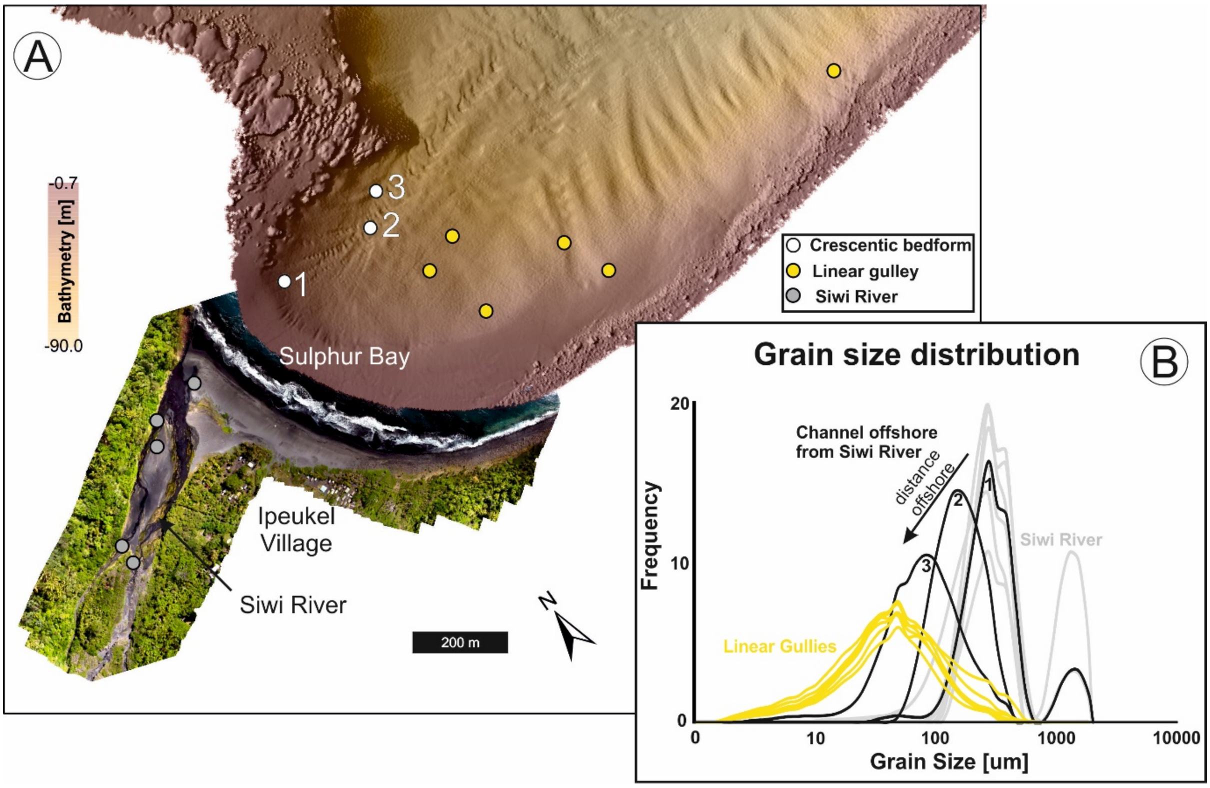

Figure 7: Location of sediment samples presented in this study (A) overlain on drone-acquired photographic survey of Siwi River and multibeam bathymetry offshore. Grain size distributions (B) from Siwi River are similar to those from the proximal part of the sinuous channel with crescentic bedforms, but distinct from samples from linear gullies.

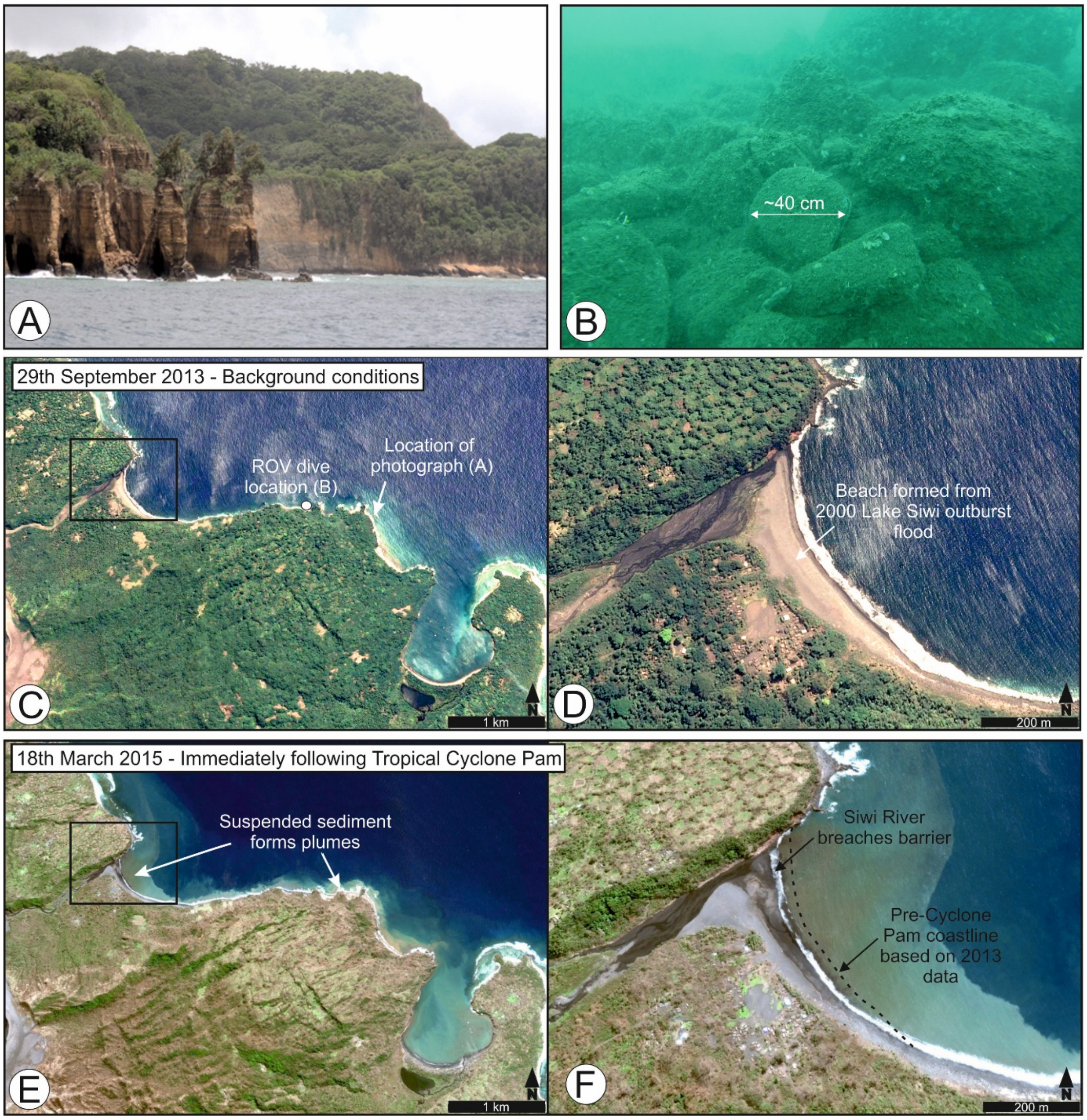

Figure 8: Photograph (A) from survey vessel of steep coastal cliffs at location annotated on (E). Photograph taken using ROV (B) showing boulders (~30-50 cm in diameter) below the cliffs. Satellite photography prior to (C&D) and immediately following (E&F) tropical cyclone Pam. Panels D and F zoomed in to Siwi River and Sulphur Bay. Map images acquired by NASA and exported from Google: Digital Globe.

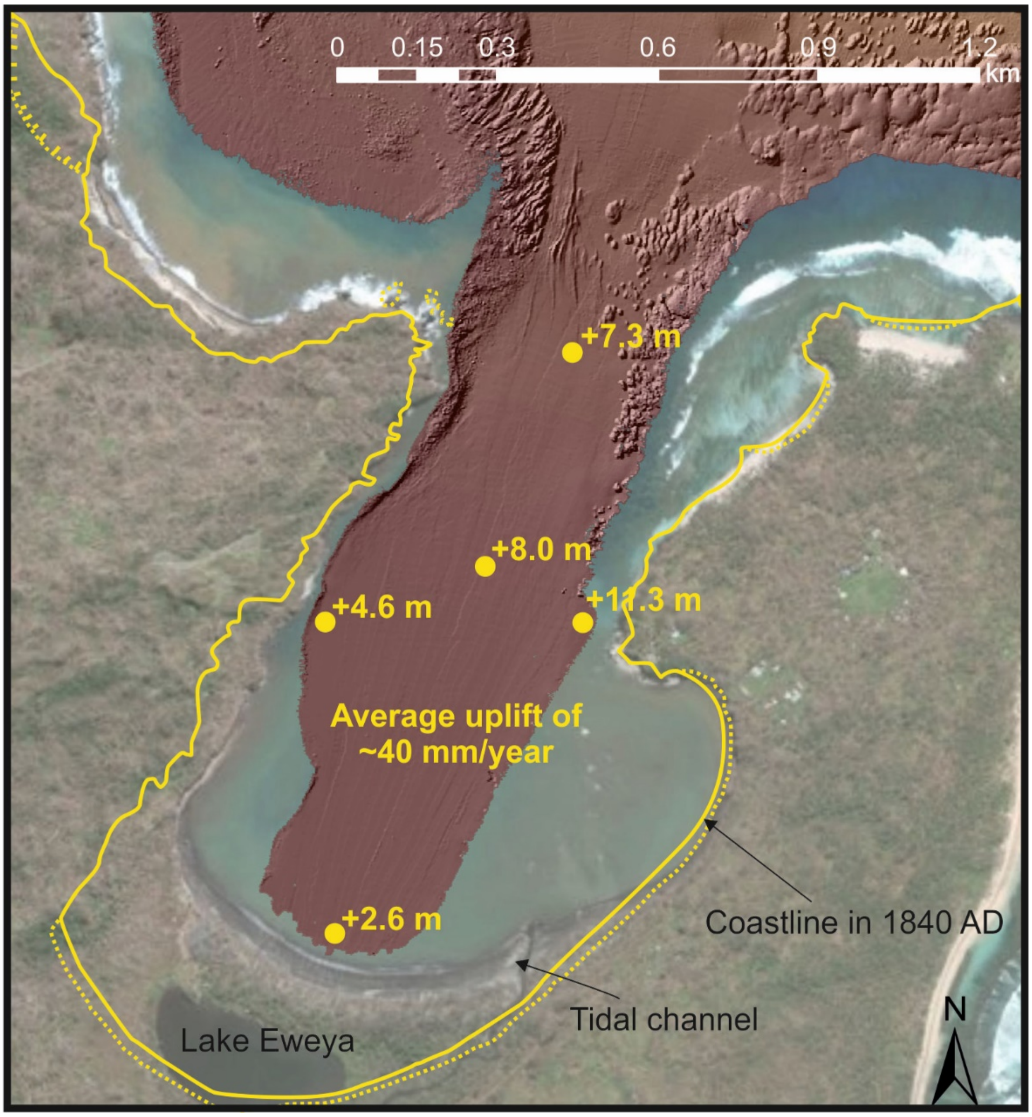

Figure 9: Comparison of satellite photography and bathymetry of Resolution Bay acquired in 2017, compared with outline of coastline from mapping by Captain Belcher in 1840 in yellow (Hydrographic Office of the Admiralty, 1843). Filled circles illustrate comparison between bathymetric soundings in 1840 and 2017, which show an average elevation difference of +6.8 m; equating to an annual average rise of 40 mm/year.

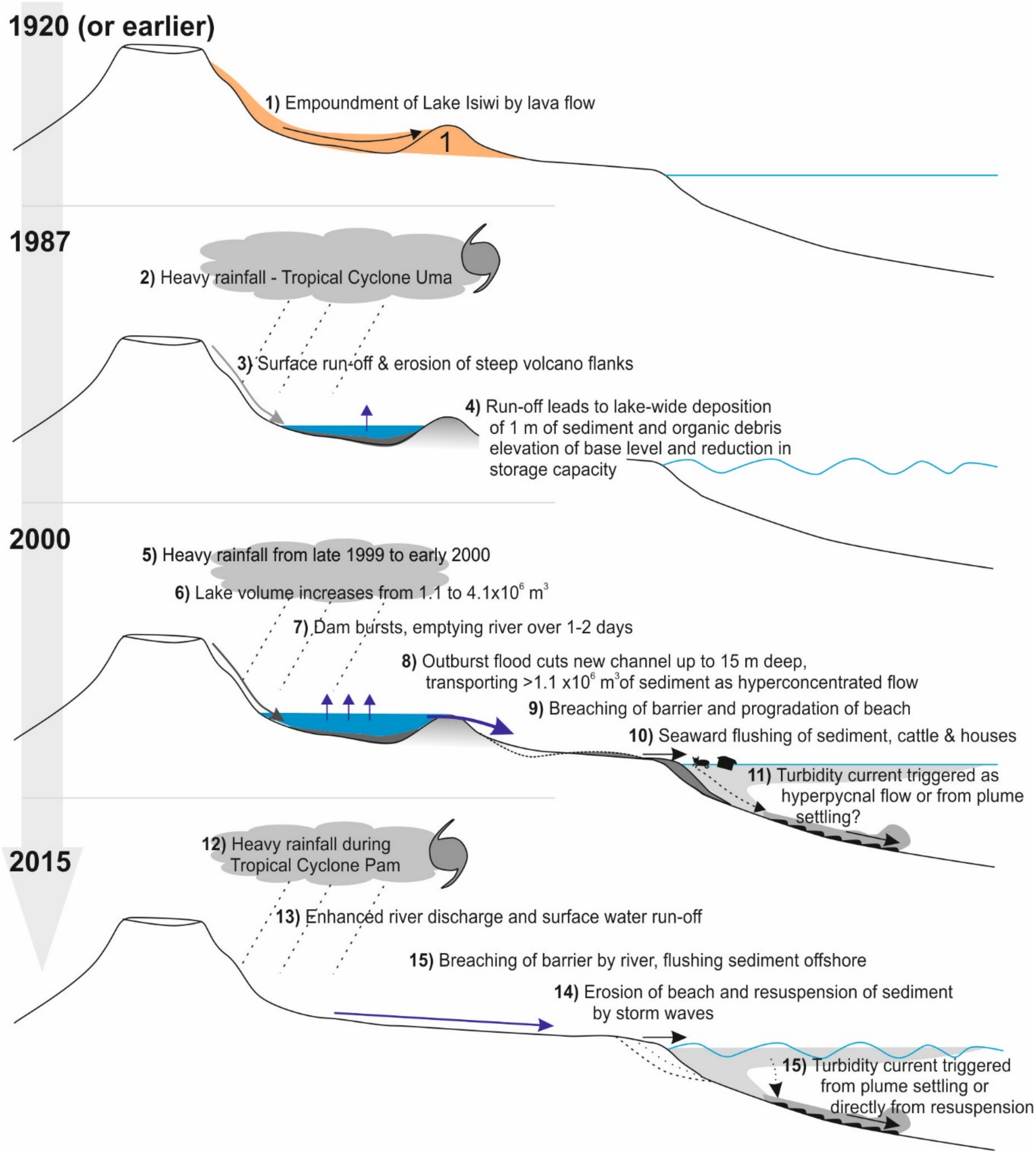

Figure 10: Sequential chain of cascading effects (from 1 to 15) that may have led to the triggering of turbidity currents that formed crescentic bedforms offshore Sulphur Bay, Tanna Island.

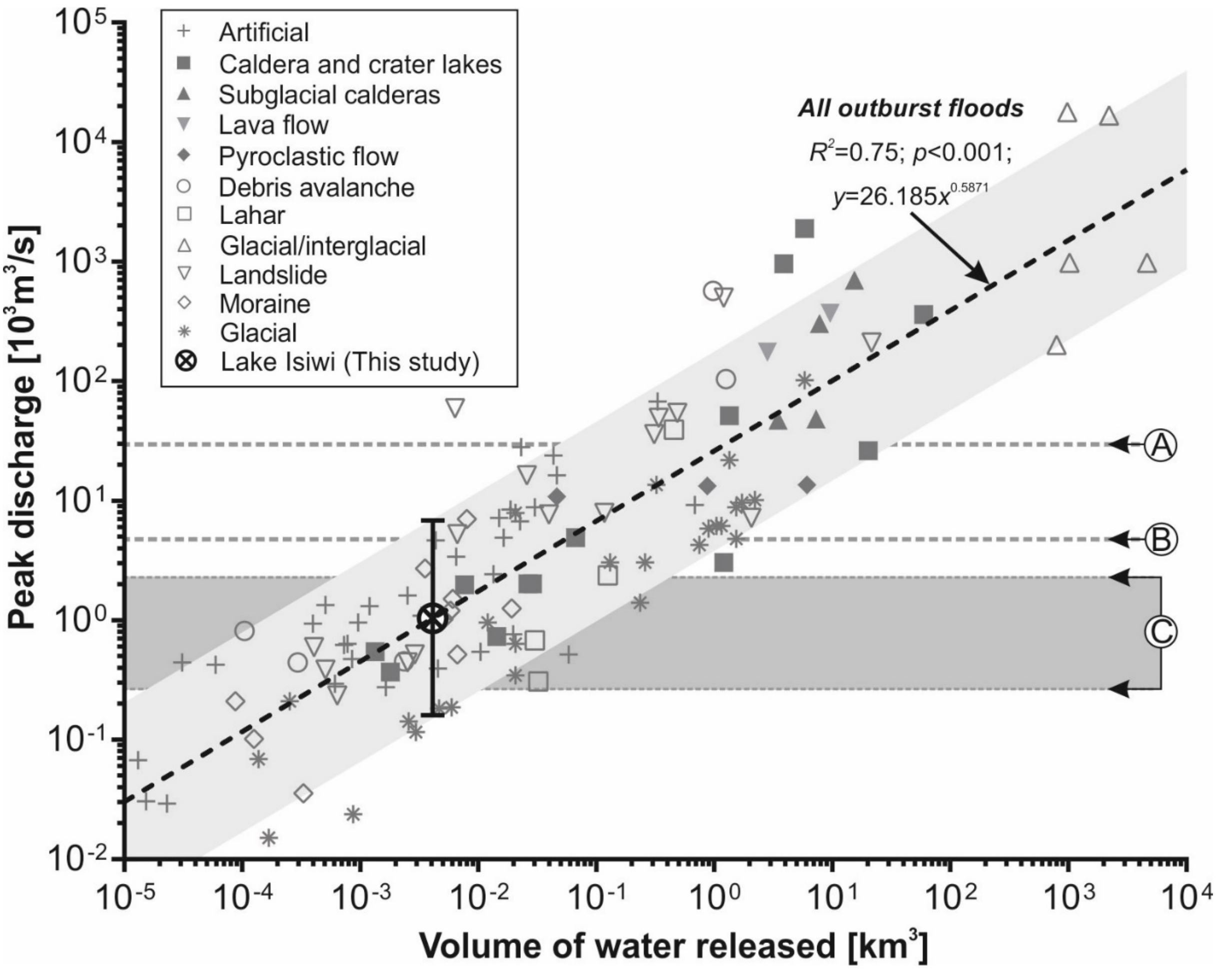

Figure 11: Plot of peak discharge in relation to volume of water released from outburst floods based on global data from Manville (2010). Black dashed lined is power-law trend for all outburst floods, and light grey parallel fill is the 99th percentile range. Lettered annotations refer to peak river discharges for: (A) Gaoping River following Typhoon Morakot in 2009 [28,000 m^3/s; Carter et al., 2014] when hyperpycnal flow triggered a turbidity current; (B) highest recorded river discharge in New Caledonia on Grand Terre due to Cyclone Anne in 1988 [4,583 m^3/s; Terry et al., 2008]; and (C and dark grey fill) the range of discharge on the Squamish River, British Columbia when turbidity currents are known to occur (Clare et al., 2017). The estimated discharge for the 2000 Lake Isiwi outburst flood is ~1000 m^3/s, with an upper bound estimate of 7000 m^3/s.

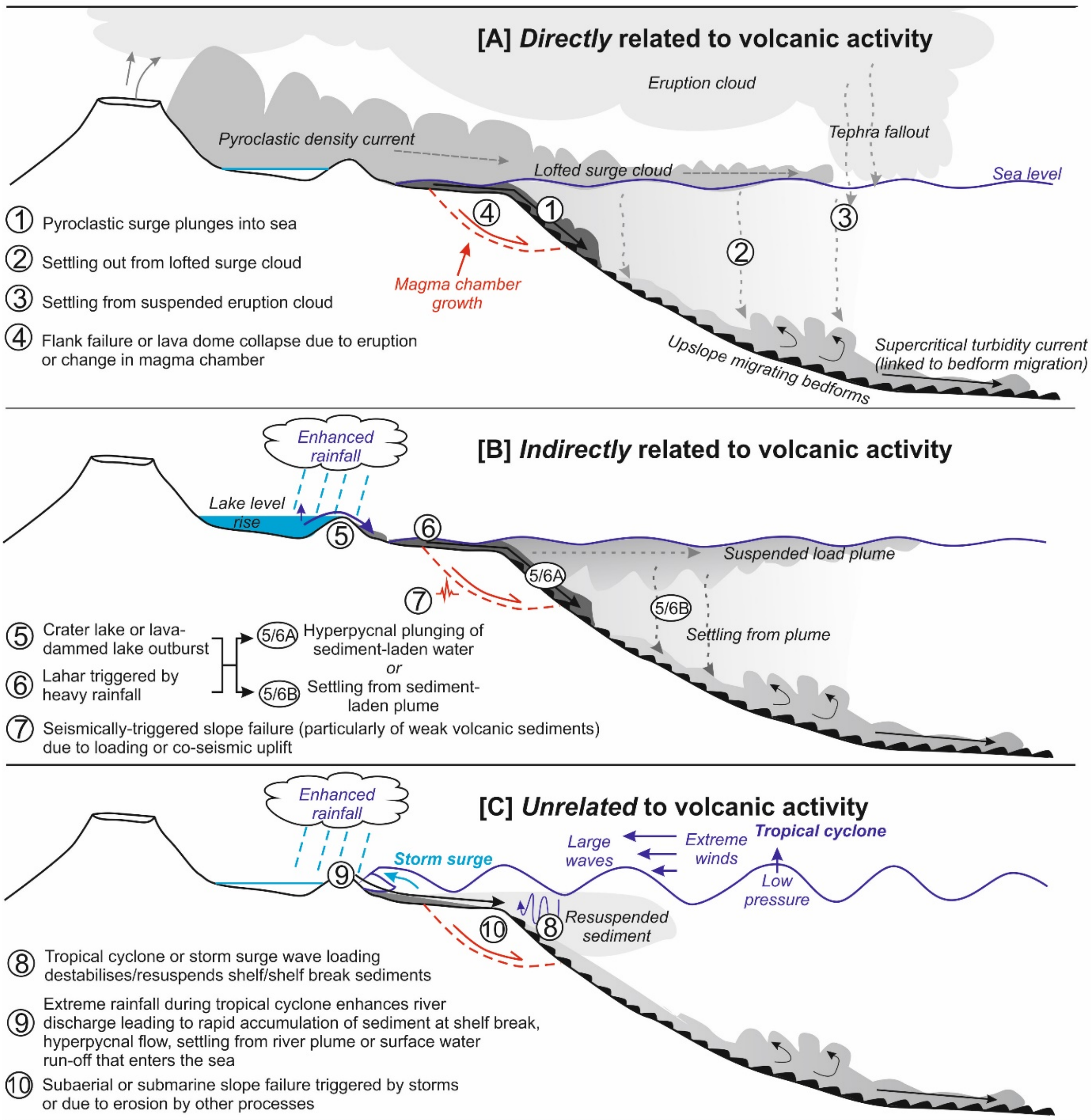

Figure 12: General model of processes that contribute to preconditioning or drive triggering of submarine slope failures and turbidity currents at volcanic islands. Unlike in Fig. 10, the numbering here is not sequential and simply refers to isolated processes.

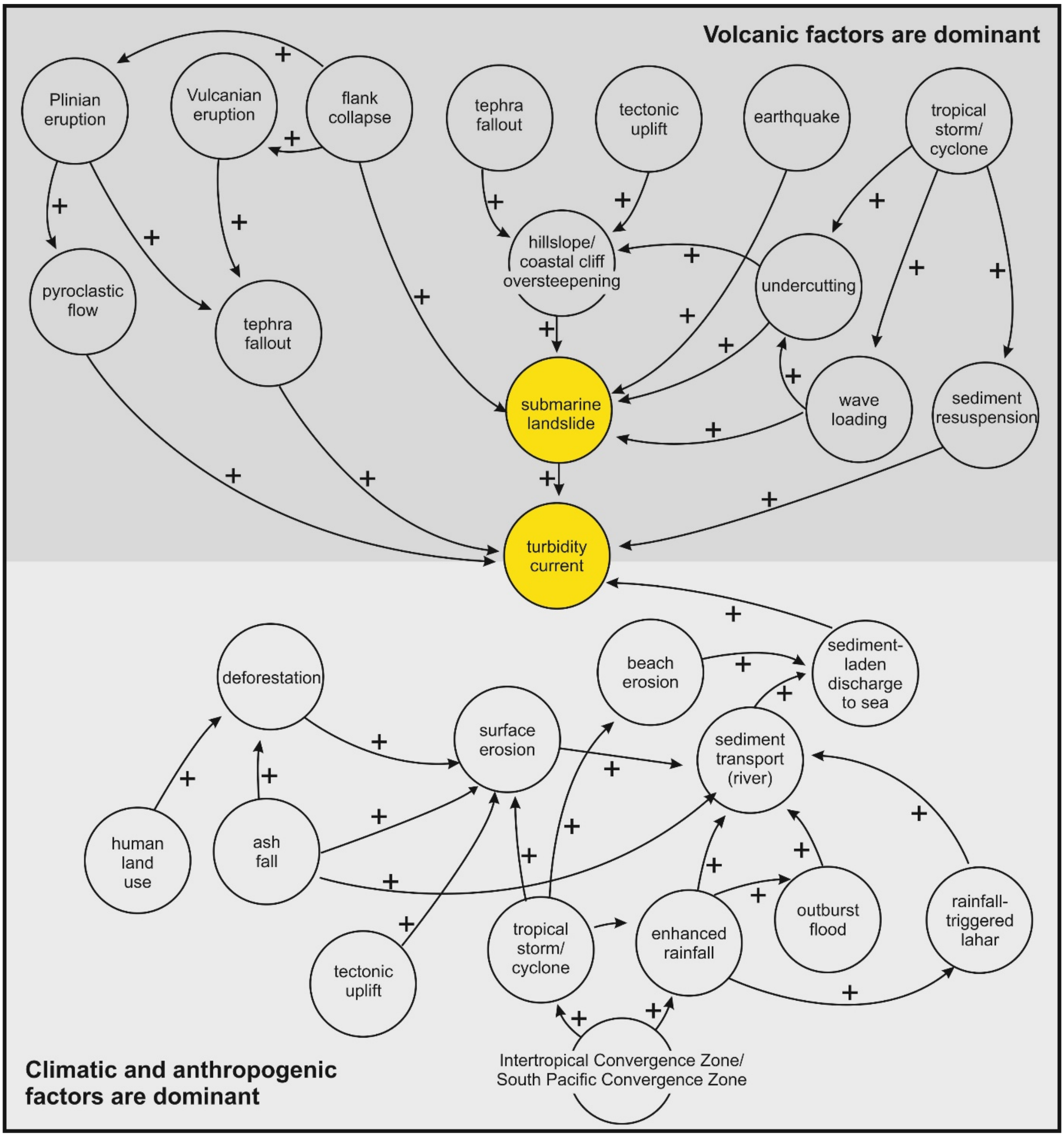

Figure 13: Illustration of the potential complexity of interacting processes at volcanic islands that may precondition and trigger submarine landslides and turbidity currents. Plus signs and arrowed lines indicate how an increase in a variable may make a subsequent process more likely. Figure shows scenarios where volcanic factors may dominate (dark grey) and where climatic or anthropogenic factors may be more important (light grey).